Geochemistry Geophysics Geosystems G3
AN ELECTRONIC JOURNAL OF THE EARTH SCIENCES
Published by AGU and the Geochemical Society

Article
Volume 9, Number 3
19 March 2008
Q03015, doi:10.1029/2007GC001795
ISSN: 1525-2027

Construction of the Galápagos platform by large submarine volcanic terraces

Dennis Geist
Department of Geological Sciences, University of Idaho, 3022, Moscow, Idaho 83844, USA (dgeist@uidaho.edu)

Bridget A. Diefenbach
Department of Geological Sciences, University of Idaho, Moscow, Idaho, USA

Now at Associated Earth Sciences, Inc., 2911 1/2 Hewitt Ave, Suite 2, Everett, Washington 98201, USA

Daniel J. Fornari
Geology and Geophysics Department, Woods Hole Oceanographic Institution, Woods Hole, Massachusetts 02543, USA (dfornari@whoi.edu)

Mark D. Kurz
Marine Chemistry and Geochemistry Department, Woods Hole Oceanographic Institution, Woods Hole, Massachusetts 02543, USA (mkurz@whoi.edu)

Karen Harpp
Department of Geology, Colgate University, Hamilton, New York 13346, USA (kharpp@mail.colgate.edu)

Jerzy Blusztajn
Geology and Geophysics Department, Woods Hole Oceanographic Institution, Woods Hole, Massachusetts 02543, USA

[1] New multibeam bathymetric and side-scan sonar data from the southwestern edge of the Galápagos platform reveal the presence of ~60 large, stepped submarine terraces between depths of 800 m and 3500 m. These terraces are unique features, as none are known from any other archipelago that share this geomorphic form or size. The terraces slope seaward at <2° and are surrounded by escarpments that average ~300 m in height with average slopes of 24°. The stepped morphology, fine-scale features, and sinuous planform continuity of terrace edges indicate that each terrace results from a sequence of major submarine volcanic eruptions, similar in extent to young deep-water (>3000 m) lava flow fields west of Fernandina and Isabela Islands. The terraces are formed of thick sequences of lava flows that coalesce to form the foundation of the Galápagos platform, on which the subaerial central volcanoes are built. The compositions of basalts dredged from the submarine terraces indicate that most lavas are chemically similar to subaerial lavas erupted from Sierra Negra volcano on southern Isabela Island. There are no regular major element, trace element, or isotopic variations in the submarine lavas as a function of depth, relative stratigraphic position, or geographic location along the southwest margin of the platform. We hypothesize that magma supply at the western edge of the Galápagos hot spot, which is influenced by both plume and mid-ocean ridge magmatic processes, leads to episodic eruption of large lava flows. These large lava flows coalesce to form the archipelagic apron upon which the island volcanoes are built.

Components: 13,408 words, 14 figures, 5 tables.

Keywords: submarine volcanism.

Index Terms: 3075 Marine Geology and Geophysics: Submarine tectonics and volcanism; 3045 Marine Geology and Geophysics: Seafloor morphology, geology, and geophysics; 1065 Geochemistry: Major and trace element geochemistry.

Received 21 August 2007; **Revised** 20 December 2007; **Accepted** 24 December 2007; **Published** 19 March 2008.

Geist, D., B. A. Diefenbach, D. J. Fornari, M. D. Kurz, K. Harpp, and J. Blusztajn (2008), Construction of the Galápagos platform by large submarine volcanic terraces, *Geochem. Geophys. Geosyst.*, *9*, Q03015, doi:10.1029/2007GC001795.

1. Introduction

[2] The subaerial geology of the Galápagos Islands has revealed fundamental petrological, volcanological, and tectonic insights related to the formation of oceanic archipelagos and, more recently, the interactions between mantle plumes and mid-ocean ridges (MORs). Despite extensive studies of the subaerial volcanoes, the early eruptive histories of Galápagos volcanoes, as reflected in the submarine archipelagic platform, have remained largely unexplored.

[3] The Galápagos archipelago is a hot spot province located south of the intermediate-spreading Galápagos Spreading Center (GSC) (Figure 1). The islands lie on the Nazca plate, which is moving at azimuth 91° in the hot spot reference frame [*Gripp and Gordon*, 2002]; thus the most active volcanoes are in the western part of the archipelago. Recent seismic studies [*Hooft et al.*, 2003; *Villagómez et al.*, 2007] show that the western Galápagos overlies a low-velocity anomaly that extends through the upper mantle at least to the bottom of the transition zone (660 km).

[4] Many aspects of the Galápagos are unusual compared to other hot spot-related archipelagos, owing to the proximity of the GSC [e.g., *Geist et al.*, 1988], and the northward drift of the spreading center relative to the hot spot since ~8 Ma when it was centered over it [*Wilson and Hey*, 1995]. Many of these anomalous features are manifested in the submarine environment. For example, the islands, which are constructed of central volcanoes, are located on top of a voluminous plateau-like platform, whose origin is unknown. Also, although the volcanoes are generally older in the east (as much as ~3 Ma and younger in the west, young lavas extend over the entire region [*White et al.*, 1993]. Finally, strong tectonic control of volcanism currently occurs in the northern part of the archipelago, between the Galápagos platform and the GSC. In this area, elongate volcanoes, fractures, and rift zones characterize the seafloor and islands; this tectonic activity is thought to result from a combination of high mantle temperatures and stresses attributable to plume-ridge interaction [*Harpp and Geist*, 2002; *Harpp et al.*, 2003; *Mittelstaedt and Ito*, 2005].

[5] Prior to the 2001 DRIFT04 cruise, most information on the submarine Galápagos region was derived from the 1990 PLUME02 cruise [*Christie et al.*, 1992] and the 2000 AHA-Nemo cruise [*Fornari et al.*, 2001]. On DRIFT04, we completed surface-towed side-scan sonar and multibeam bathymetric surveys of the entire SW perimeter of the archipelago and collected dredged rock samples [*Kurz et al.*, 2001a, 2001b; *Fornari et al.*, 2001; *Harpp et al.*, 2003; *Geist et al.*, 2005, 2006] (Figures 1 and 2). The bathymetric and side-scan data reveal that the submarine margins of the western and southern edges of the platform consist of volcanic rift zone ridges extending from subaerial volcanoes, lava flow fields on the deep seafloor, and large volcanic constructional submarine terraces [*Geist et al.*, 2006; *Harpp et al.*, 2003; *Diefenbach*, 2004; *Glass et al.*, 2007] (Figure 2c and Tables 1 and 2). This study presents the results of an extensive field and analytical program focused on the SW margin of the Galápagos platform to assess the mechanisms of platform construction and evolution of the archipelagic apron.

2. Methods

[6] Side-scan sonar data acquisition was carried out using the Hawaii Mapping Research Group's HAWAII MR1 towed system [*Rongstad*, 1992; *Davis et al.*, 1993], which yields 8 m pixel resolution backscatter data (Figure 2b). Multibeam bathymetry was acquired using the Simrad EM-120 system on R/V *Revelle* supplemented by

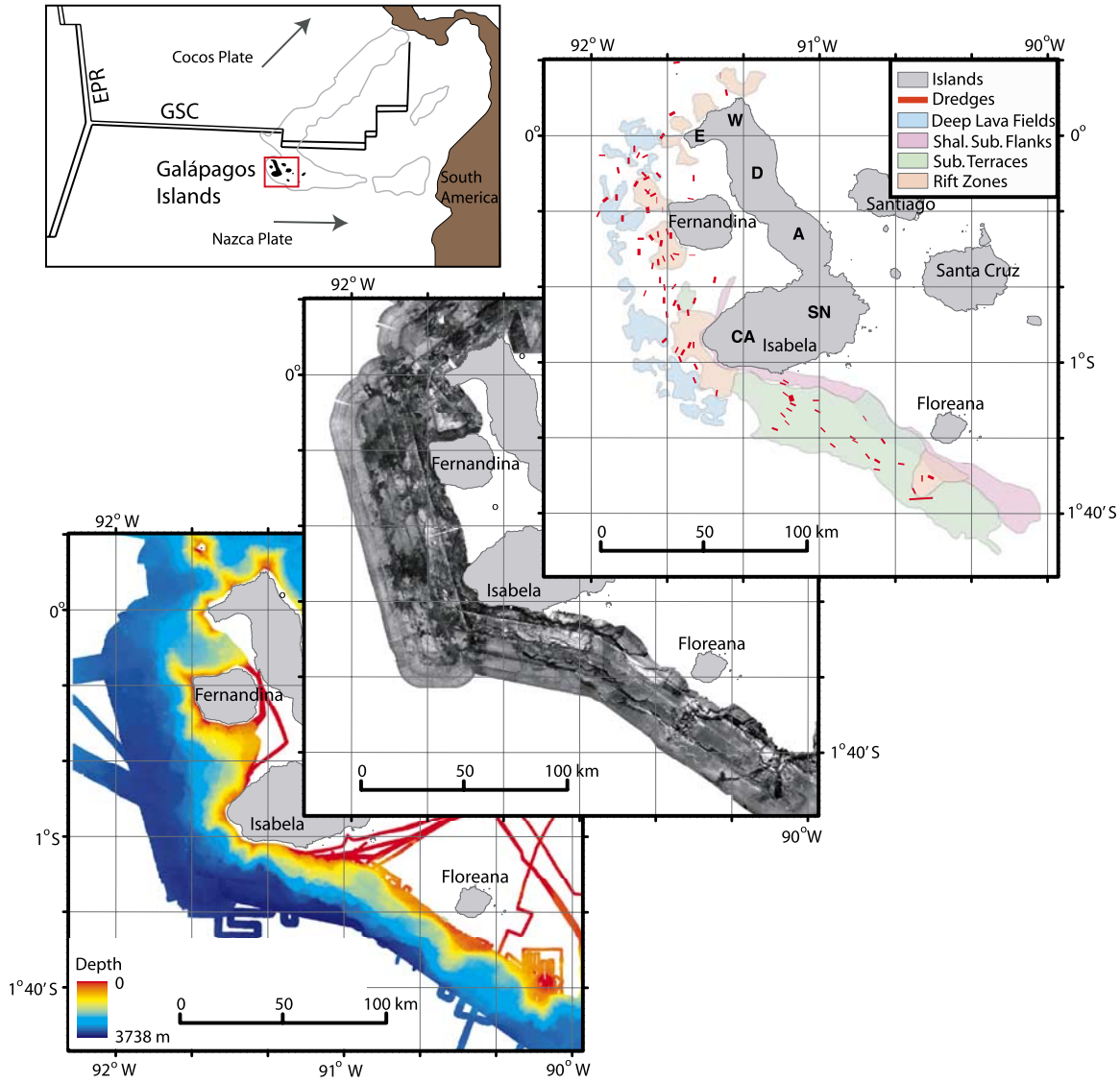

Figure 1. (top left) Regional setting of Galápagos archipelago, showing Galápagos Spreading Center (GSC), East Pacific Rise (EPR), and hot spot tracks forming the Cocos and Carnegie Ridges (gray lines). (top right) Regional geologic map of the submarine Galápagos [from *Geist et al.*, 2006] showing dredge locations. Individual volcanoes on Isabela Island are CA, Cerro Azul; SN, Sierra Negra; A, Alcedo; D, Darwin; W, Wolf, and E, Ecuador. (middle) Regional MR1 side-scan sonar image from Drift04 cruise in 2001 (high backscatter is gray to black). (bottom) Regional multibeam bathymetric map.

previous multibeam data collected in the area (Figure 2a). Final bathymetry grids were produced at 80 m horizontal resolution. Data collected from ship's navigation and compass in the MR1 tow-fish were used to compute a compass correction, which was applied to the navigation input for all MR1data. Initial acoustic phase-angle to nadir-angle tables were produced from data collected over the flat seafloor. Post-processing of acoustic imagery data was done on an ongoing basis throughout the survey and merged with navigation data collected from shipboard P-code GPS. Detailed inspection of merged bathymetric and side-scan maps indicates that they are geodetically coregistered to within the accuracy of the bathymetric grid (Figure 3).

[7] Bathymetry and side-scan sonar data were analyzed using a geographic information system and 3-D visualization software. Individual terraces are defined as areas with continuous sub-horizontal surfaces, bound by escarpments at least 50 m tall. Each terrace has a sinuous seaward edge, and contact relationships between adjacent terraces at

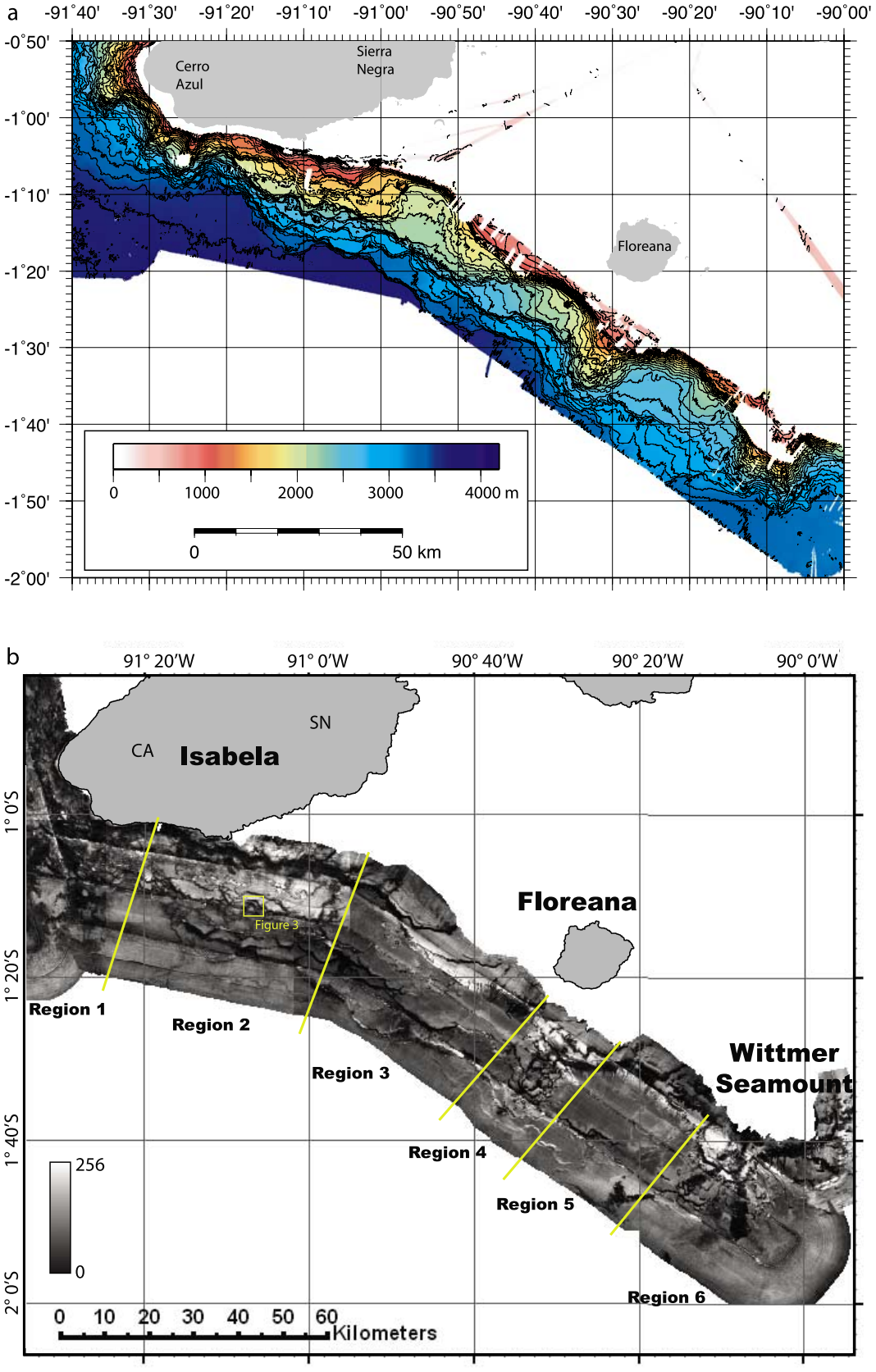
a
-91°40' -91°30' -91°20' -91°10' -91°00' -90°50' -90°40' -90°30' -90°20' -90°10' -90°00'
-0°50'
-1°00'
-1°10'
-1°20'
-1°30'
-1°40'
-1°50'
-2°00'
Cerro Azul
Sierra Negra
Floreana
0 1000 2000 3000 4000 m
0 50 km
b
91° 20'W 91° 0'W 90° 40'W 90° 20'W 90° 0'W
1° 0'S
1° 20'S
1° 40'S
2° 0'S
SN
CA
Isabela
Floreana
Figure 3
Region 1
Region 2
Region 3
Region 4
Region 5
Region 6
Wittmer Seamount
256
0
0 10 20 30 40 50 60 Kilometers

Figure 2

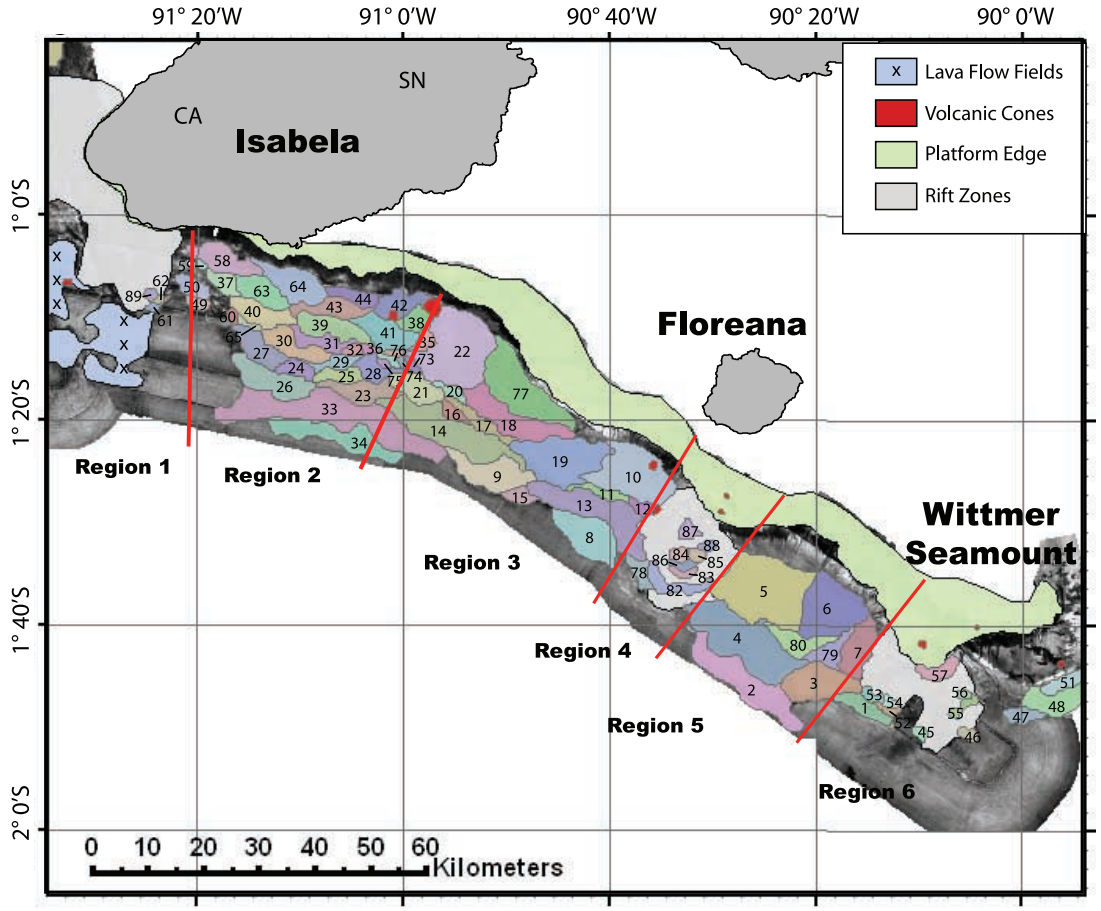

Figure 2. (continued)

similar depth intervals provide limited means to determine relative ages between terraces (Figure 2c and Tables 1 and 2). The terraces are numbered for discussion, and there is no geological/temporal meaning to the numbers.

[8] The sampling program on the SW Galápagos terraces conducted during DRIFT04 consisted of 25 dredges (Figures 1 and 4). Results from other dredges on the western margin of the platform adjacent to Fernandina volcano, Genovesa Ridge, and the northern platform margin adjacent to Wolf volcano have been reported by *Geist et al.* [2005, 2006] and *Harpp et al.* [2003]. All dredges along the SW margin of the platform yielded igneous material. Rocks were rinsed with fresh water, described, and sub-samples of glass chips were removed from representative rocks for geochemical analysis.

[9] Fifty-one glass and nine whole rock samples were analyzed for major element composition by electron microprobe and X-ray fluorescence at the Geoanalytical Laboratory at Washington State University. A Cameca Camebax electron microprobe was used to analyze glass samples for major elements with an acceleration voltage of 15 kV and a beam current of 12.6 nA. A defocused beam

Figure 2. (a) Multibeam bathymetric map of the SW Galápagos platform. Contour interval is 100 m. (b) MR-1 side-scan sonar map with 8 m pixel resolution. Light areas have low acoustic reflectivity, and dark regions indicate high backscatter. Yellow lines show boundaries of different regions discussed in the text. Box outlines area of Figure 3. (c) Geologic interpretation of side-scan sonar and bathymetry data with individual terraces numbered and indicated by different colors (numbering does not reflect any age sequence). Volcanic cones are shown in red, the platform edge is in light green, volcanic ridges are in light gray, and lava flow fields are in light blue with "x" symbols. Red lines show boundaries of different regions discussed in the text. Mapping was completed using the geospatial capabilities of ArcGIS™. For all images, islands are shown in gray. CA, Cerro Azul; SN, Sierra Negra.

Table 1. Individual Terrace Dimensions[a]

Terrace Location	Terrace Number	Width, km	Length, km	Exposed Surface Area, km^2	Scarp Height, m	Minimum Est. Vol., km^3	Plateau Slope, m/km	Plateau Slope, deg	Scarp Slope, deg
Region 1	89	2	2	4.00					
Region 1	61	2	3	3.39					
Region 1	62	2	3	2.78					
Region 2	33	6	42	194.04					
Region 2	34	5	25	77.34					
Region 2	26	5	15	61.68	200	12.34	5.53	0.55	20
Region 2	64	6	15	57.00					
Region 2	58	5	15	47.05	467	21.96	22.49	2.25	21
Region 2	41	5	13	46.62	317	14.76	1.28	0.13	23
Region 2	39	4	15	44.84	380	17.04	15.94	1.59	24
Region 2	23	5	15	41.99	527	22.12	0.72	0.07	26
Region 2	30	5	14	40.35	400	16.14	13.76	1.38	26
Region 2	40	3	13	39.09	507	19.81	12.97	1.30	32
Region 2	27	4	11	38.78	497	19.26	13.52	1.35	25
Region 2	63	5	11	37.90					
Region 2	21	5	11	37.19	330	12.27	4.24	0.42	18
Region 2	43	4	15	35.05	40	1.40	42.08	4.21	19
Region 2	42	5	11	35.03	147	5.14	15.63	1.56	15
Region 2	31	3	10	25.84	327	8.44	13.50	1.35	24
Region 2	28	6	8	24.46	303	7.42	7.56	0.76	19
Region 2	44	3	10	20.62	413	8.52	21.93	2.19	23
Region 2	25	2	8	19.81					
Region 2	38	4	6	18.56	208	3.87	5.18	0.52	17
Region 2	50	3	7	17.98	330	5.93	29.69	2.97	23
Region 2	37	4	8	17.73	273	4.85	19.09	1.91	23
Region 2	29	3	9	17.21	293	5.05	2.31	0.23	21
Region 2	24	3	7	17.18					
Region 2	35	3	5	17.17					
Region 2	49	2	5	8.76	400	3.51	13.65	1.36	27
Region 2	32	2	4	6.83	293	2.00	4.42	0.44	21
Region 2	73	2	4	5.21					
Region 2	65	1	5	5.01					
Region 2	76	1	5	4.97					
Region 2	36	2	4	4.64	310	1.44	29.52	2.95	24
Region 2	60	2	3	4.53					
Region 2	75	2	3	3.53					
Region 2	59	1	2	3.13					
Region 2	74	1	2	3.11					
Region 3	22	14	11	148.61	280	41.61	11.79	1.18	33
Region 3	14	5	29	122.04	383	46.78	15.94	1.59	26
Region 3	10	9	15	113.34	368	41.75	25.71	2.57	27
Region 3	77	6	23	112.24					
Region 3	19	9	17	109.44	333	36.48	21.96	2.20	29
Region 3	13	5	25	107.53	393	42.29	19.88	1.99	31
Region 3	18	4	22	78.12	310	24.22	14.36	1.44	18
Region 3	8	7	16	71.40					
Region 3	9	6	15	65.59	225	14.76	16.70	1.67	21
Region 3	17	3	14	23.78	450	10.70	18.79	1.88	29
Region 3	78	4	8	16.10					
Region 3	11	2	11	14.02					
Region 3	15	3	7	13.33	142	1.89	14.74	1.47	15
Region 3	16	3	7	11.63					
Region 3	20	2	7	10.60					
Region 3	12	4	5	10.08	463	4.67	20.57	2.06	32
Region 4	82	2	11	26.57					
Region 4	87	3	3	9.12					
Region 4	84	3	4	8.42					
Region 4	83	1	5	7.07					
Region 4	86	1	5	6.65					
Region 4	85	2	3	6.60					

Table 1. (continued)

Terrace Location	Terrace Number	Width, km	Length, km	Exposed Surface Area, km^2	Scarp Height, m	Minimum Est. Vol., km^3	Plateau Slope, m/km	Plateau Slope, deg	Scarp Slope, deg
Region 4	88	2	3	4.90					
Region 5	5	13	16	171.30	340	58.24	11.63	1.16	22
Region 5	4	7	22	151.00					
Region 5	2	5	25	104.48					
Region 5	6	12	11	100.08					
Region 5	3	7	14	69.64					
Region 5	7	5	11	48.25					
Region 5	80	4	10	33.40					
Region 5	79	4	9	26.22					
Region 5	1	3	11	25.20					
Region 6	48	4	15	52.80					
Region 6	51	2	12	33.98					
Region 6	57	3	8	19.47					
Region 6	47	4	8	16.74					
Region 6	55	2	6	8.71					
Region 6	53	2	4	7.21					
Region 6	46	2	4	7.13					
Region 6	52	1	5	6.30					
Region 6	45	2	3	5.35					
Region 6	54	2	3	4.93					
Region 6	56	2	2	3.79					

[a] Terrace numbers are shown in Figure 2c. Terrace dimensions were calculated using ArcGIS (http://www.esri.com). Scarp height, minimum volume estimates, plateau slope, and scarp slope could not be measured accurately for all terraces due to overlap and steep slopes which obscure the basal depth of some terraces.

was used, and sodium intensity was monitored as a function of time and corrected for volatilization. For most samples, two points were measured on three separate glass shards from the same sample. The results are averages of the analyses (Table 3). When glass was not available, major element analyses of whole rock samples were determined by X-ray fluorescence (methods and accuracy reported by *Johnson et al.* [1999] and precision reported in Table 3). Trace element concentrations of hand picked glasses were measured on a subset of 18 samples by inductively coupled plasma-mass spectrometry (ICP-MS) using a Hewlett-Packard HP4500 instrument at Colgate University (Table 4). Sample preparation and analytical techniques are described by *Harpp et al.* [2003].

[10] Strontium, neodymium, and lead isotopic analyses of 30 samples were conducted at the Woods Hole Oceanographic Institution (Table 5). Of the 30 samples, 25 are basalt chip fractions, 4 are glasses, and 1 is an olivine separate. Prior to dissolution, samples were leached for 1 hour in 6N HCl. Conventional ion-exchange procedures were used, and isotope ratios measured with a Thermo-Finnigan NEPTUNE multicollector inductively coupled plasma-mass spectrometer. The internal precision for Sr and Nd isotopic measurements is 5–10 ppm (2σ). The external precision, after

Table 2. Summary of Terrace Statistics per Region[a]

	Total Terraces	Length, km	Width, km	Surface Area, km^2	Scarp Height, m	Minimum Est. Vol., km^3	Plateau Slope, m/km	Plateau Slope, deg	Scarp Slope, deg
Region 1	3	2–3	2	3–4					
Region 2	35	2–42	1–6	3–194	40–527	1–22	1–42	<4.21	15–32
Region 3	16	5–29	2–14	10–149	142–463	2–47	14–26	<2.57	15–33
Region 4	7	3–11	1–3	5–27					
Region 5	9	9–25	3–13	25–171	340	58	12	<1.16	22
Region 6	11	2–15	1–4	4–53					

[a] Morphologic statistics have been summarized from Table 1. Scarp height, minimum volume estimates, plateau slope, and scarp slope could not be measured accurately for terraces in Regions 1, 4, and 6 due to overlap and steep slopes which obscure the basal depth of the terraces. Scarp height, minimum volume estimates, plateau slope, and scarp slope data for Regions 2, 3, and 5 represent the range of terrace dimensions that could be measured accurately.

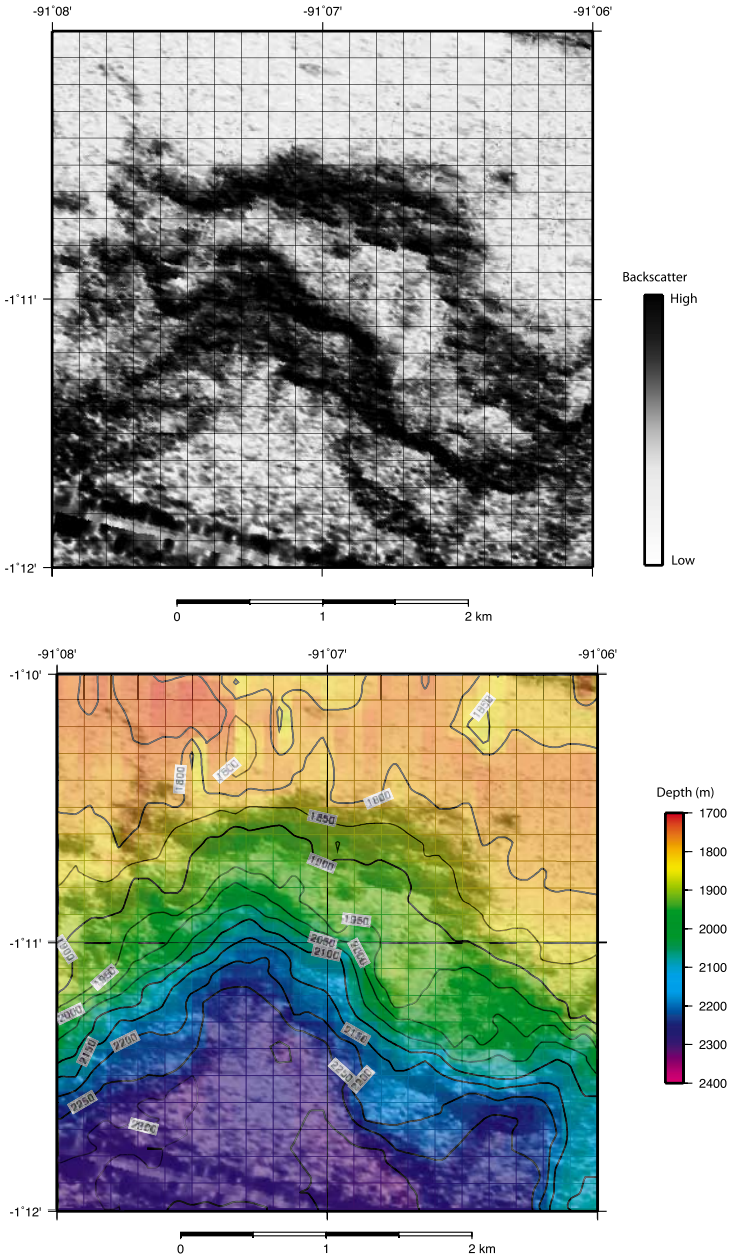

Figure 3. (top) Detailed side-scan sonar image of the scarp between terraces 31 and 39. Note the lobate structure of the three primary steps that comprise the scarp face. This morphology is consistent with the scarp being a constructional volcanic feature and not a fault scarp. (bottom) Side-scan sonar image laid over bathymetric map. Note the close registration between the backscatter reflectivity and breaks in slope. Side-scan and multibeam bathymetric coregistration is accurate to within <100 m.

correction to values for NBS987 (.710240) and La Jolla standards (.511847), is approximately 25 ppm for Sr and 15 ppm for Nd (2σ). Strontium isotopic corrections for potential Rb and Kr interferences are described by *Jackson and Hart* [2006, supplementary material]. Lead isotopic ratios have internal precision of 15–60 ppm for $^{206}Pb/^{204}Pb$, $^{207}Pb/^{204}Pb$, and $^{208}Pb/^{204}Pb$; external reproducibility ranges from 17 ppm (2σ) for $^{207}Pb/^{206}Pb$ to 117 ppm (2σ) for $^{208}Pb/^{204}Pb$. As a verification of the Pb procedure, two USGS standards were analyzed, yielding good agreement with literature values. The averages for AGV-1 were $^{206}Pb/^{204}Pb = 18.9414$, $^{207}Pb/^{204}Pb = 15.6548$, and $^{208}Pb/^{204}Pb = 38.5615$; averages for BCR-1 were $^{206}Pb/^{204}Pb = 18.8215$, $^{207}Pb/^{204}Pb = 15.6356$, and $^{208}Pb/^{204}Pb = 38.7309$.

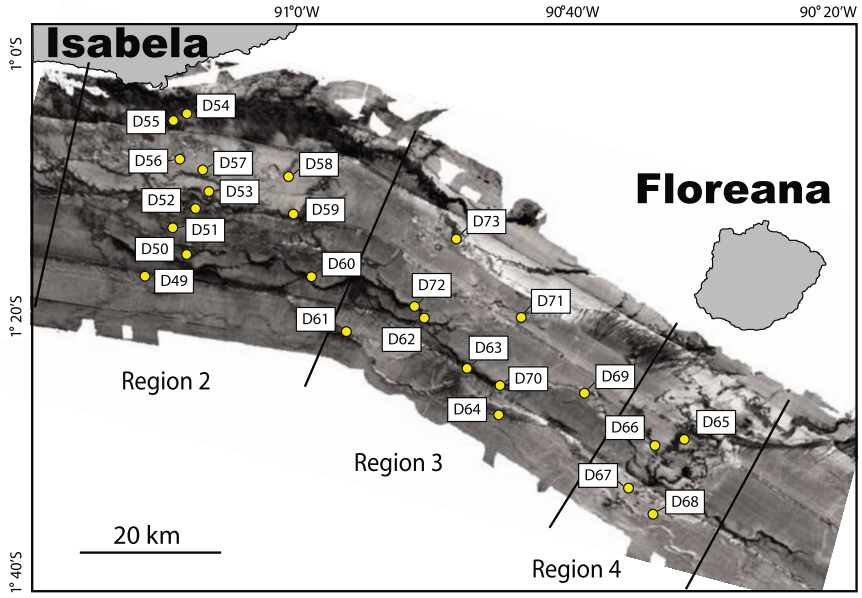

Figure 4. Side-scan sonar image of dredge locations and sample numbers. Samples D49 through D57 in Region 2 define the stratigraphic section of Figure 12.

Further details regarding isotope analytical procedures are given by *Hart and Blusztajn* [2006].

3. Morphology of the SW Galápagos Platform

[11] The SW margin of the Galápagos platform comprises six regions, which we have delineated on the basis of differences in acoustic reflectivity, morphology, and location with respect to the subaerial volcanoes (Figures 2 and 5 and Tables 1 and 2) [*Fornari et al.*, 2001; *Diefenbach*, 2004].

3.1. Region 1: Cerro Azul Ridges

[12] Two prominent ridges extend south and southwest from Cerro Azul volcano on Isabela Island (Figures 2, 5, and 6a). The ridges have a mottled backscatter texture and are interpreted to be predominantly constructional volcanic terrain comprising pillow flows and mounds with fewer sheet or lobate lavas (points b and c in Figure 6a). This interpretation is based on the abundance of pillows in the dredges and similar sonar textures in submarine volcanic terrains where visual or photographic observations have been made [e.g., *Chadwick and Embley*, 1994; *White et al.*, 2002; *Fornari et al.*, 2004; *Escartín et al.*, 2007]. Cerro Azul's submarine ridges have steep axial crests with slopes of 191 m/km and 203 m/km, steeper than Fernandina's NW submarine rift (161 m/km) and rift zones that extend seaward from other ocean island volcanoes (e.g., 73 m/km for Kilauea's Puna Ridge, and 43 m/km for Genovesa Ridge) [*Geist et al.*, 2006; *D. Smith et al.*, 2002; *Harpp et al.*, 2003].

[13] Much of the deep seafloor (below ~3400 m) south of the two ridges has low acoustic reflectivity (light gray to white in the images), which we interpret to result from a covering of >1 m of sediment. Areas of high backscatter (dark regions in the side-scan sonar images) in the flat, deep-water areas to the southwest of the ridges are interpreted to be young lava flows with thin sediment cover (point a in Figure 6a). Similar deep-water lava flows are present in the area west of Fernandina, where they are significantly more abundant [*Geist et al.*, 2006; *Glass et al.*, 2007].

3.2. Region 2: Stacked Terraces South of Isabela

[14] Thirty-five large terraces form the SW platform margin directly south of Isabela Island, in water depths ranging from >3600 m to ~1000 m (Figures 2 and 5). Escarpments separating the terrace margins range from 50 m to 530 m in height and have slopes from 15° to 32° (Tables 1 and 2). The uppermost escarpment is particularly steep and tall (~950 m) and has a scalloped margin that is concave toward the SW in plan view. The terrace surfaces slope down to the southwest,

Table 3. Major Element Contents of Dredged Lavas[a]

Sample	Location	Depth, m	Latitude, deg S	Minutes	Longitude, deg W	Minutes	SiO_2	TiO_2	Al_2O_3	FeO*	CaO	MgO	MnO	K_2O	Na_2O	P_2O_5	Mg#
Glasses																	
D49A	Region 2	3504	1	17.94	91	11.84	48.41	3.48	13.78	13.74	10.34	5.34	0.25	0.62	3.29	0.46	41
D49B	Region 2	3504	1	17.94	91	11.84	48.43	3.41	13.79	13.64	10.44	5.47	0.17	0.61	3.31	0.40	42
D49C	Region 2	3504	1	17.94	91	11.84	48.05	3.52	13.65	14.06	10.47	5.35	0.20	0.64	3.31	0.43	40
D49E	Region 2	3504	1	17.94	91	11.84	48.27	3.48	13.75	13.97	10.30	5.28	0.25	0.63	3.27	0.48	40
D49F	Region 2	3504	1	17.94	91	11.84	48.23	3.49	13.70	13.83	10.42	5.38	0.17	0.62	3.29	0.58	41
D50A	Region 2	3320	1	16.06	91	8.61	48.58	4.23	13.18	14.23	9.59	5.13	0.22	0.71	3.24	0.46	39
D51A	Region 2	2810	1	14.09	91	9.74	48.68	3.59	13.51	13.52	10.40	5.56	0.23	0.69	2.92	0.57	42
D51B	Region 2	2810	1	14.09	91	9.74	48.55	3.54	13.66	13.46	10.26	5.51	0.19	0.70	3.18	0.49	42
D51C	Region 2	2810	1	14.09	91	9.74	48.84	3.67	13.59	13.06	10.33	5.51	0.20	0.69	3.24	0.45	43
D52 burlap	Region 2	2458	1	12.69	91	8.09	48.66	3.39	13.40	12.53	11.53	6.24	0.19	0.55	3.09	0.36	47
D52*	Region 2	2458	1	12.69	91	8.09	48.39	3.32	13.46	12.84	11.58	6.14	0.20	0.55	3.02	0.39	46
D53A	Region 2	2086	1	11.34	91	7.09	50.13	3.47	13.26	13.15	9.76	5.17	0.23	0.79	3.25	0.42	41
D53B	Region 2	2086	1	11.34	91	7.09	49.40	4.18	13.11	13.83	9.49	5.04	0.22	0.76	3.20	0.43	39
D53C	Region 2	2086	1	11.34	91	7.09	50.27	3.43	13.32	13.13	9.56	5.22	0.22	0.75	3.34	0.42	41
D53D	Region 2	2086	1	11.34	91	7.09	50.21	3.38	13.44	13.13	9.53	5.29	0.17	0.72	3.24	0.57	42
D55A	Region 2	1000	1	5.88	91	9.69	48.38	2.69	14.51	11.71	11.59	6.47	0.16	0.54	3.06	0.44	50
D55B	Region 2	1000	1	5.88	91	9.69	48.68	2.70	14.34	11.68	11.62	6.51	0.18	0.57	3.07	0.35	50
D55C	Region 2	1000	1	5.88	91	9.69	48.50	2.72	14.21	11.97	11.44	6.58	0.22	0.59	3.07	0.32	49
D55D	Region 2	1000	1	5.88	91	9.69	48.55	2.69	14.19	11.95	11.60	6.49	0.17	0.58	3.04	0.36	49
D55G	Region 2	1000	1	5.88	91	9.69	48.35	2.74	14.35	11.99	11.68	6.41	0.19	0.56	2.95	0.29	49
D56A	Region 2	1444	1	8.51	91	9.07	48.65	3.59	13.46	13.20	10.52	5.87	0.19	0.63	3.08	0.47	44
D56C	Region 2	1444	1	8.51	91	9.07	48.57	3.63	13.37	13.44	10.55	5.86	0.22	0.65	3.01	0.45	44
D56E	Region 2	1444	1	8.51	91	9.07	48.97	3.61	13.43	12.96	10.71	5.96	0.20	0.63	3.03	0.49	45
D57A	Region 2	1633	1	9.68	91	7.99	48.50	3.69	13.32	13.45	10.40	5.74	0.20	0.60	3.07	0.57	43
D57B	Region 2	1633	1	9.68	91	7.99	48.54	3.70	13.31	13.38	10.33	5.73	0.21	0.58	3.05	0.57	43
D57C	Region 2	1633	1	9.68	91	7.99	48.63	3.71	13.38	13.44	10.41	5.74	0.17	0.58	3.06	0.58	43
D57D	Region 2	1633	1	9.68	91	7.99	48.62	3.71	13.48	13.39	10.42	5.80	0.21	0.58	2.99	0.52	44
D57E	Region 2	1633	1	9.68	91	7.99	48.62	3.69	13.45	13.50	10.44	5.77	0.17	0.58	3.04	0.41	43
D58A	Region 2	1563	1	10.28	91	0.95	48.81	3.58	13.78	12.62	10.63	5.96	0.20	0.56	3.07	0.39	46
D58 burlap	Region 2	1563	1	10.28	91	0.95	49.16	3.61	13.54	12.56	10.88	5.81	0.19	0.58	3.06	0.43	45
D59A	Region 2	1897	1	13.09	91	0.64	48.71	3.09	14.03	12.40	11.13	6.20	0.14	0.54	2.95	0.38	47
D60A	Region 2	3117	1	17.97	90	59.23	49.54	3.01	14.09	11.95	10.82	6.19	0.20	0.54	3.03	0.36	48
D61	Region 3	3440	1	22.13	90	56.68	48.85	4.13	13.33	14.14	9.99	5.01	0.25	0.65	2.94	0.58	39
D62	Region 3	2607	1	21.08	90	50.69	50.01	3.59	13.83	11.90	10.52	5.60	0.31	0.68	3.05	0.27	46
D63	Region 3	3002	1	24.95	90	47.47	48.65	2.78	14.40	11.64	11.78	6.63	0.17	0.44	2.93	0.30	50
D64C	Region 3	3358	1	28.58	90	44.95	50.09	2.96	15.01	11.69	10.82	5.64	0.18	0.61	2.39	0.32	46
D64D	Region 3	3358	1	28.58	90	44.95	49.50	2.99	14.73	11.90	10.85	5.63	0.11	0.58	3.08	0.30	46
D64E	Region 3	3358	1	28.58	90	44.95	49.55	2.98	14.66	11.84	10.88	5.60	0.17	0.57	3.05	0.39	46
D69A	Region 3	2425	1	27.10	90	38.54	49.74	2.80	14.21	11.54	11.17	6.28	0.20	0.56	2.89	0.29	49
D70C	Region 3	2811	1	26.34	90	44.98	49.25	3.35	13.68	13.23	10.66	5.67	0.24	0.57	3.07	0.33	43
D70D	Region 3	2811	1	26.34	90	44.98	49.07	3.32	13.63	13.24	10.61	5.64	0.20	0.56	2.99	0.34	43
D70E	Region 3	2811	1	26.34	90	44.98	49.47	2.53	14.41	11.05	11.84	6.82	0.19	0.45	2.66	0.27	52
D70I	Region 3	2811	1	26.34	90	44.98	49.24	3.31	13.75	12.97	10.49	5.65	0.22	0.56	3.04	0.38	44
D72A	Region 3	2415	1	20.18	90	51.39	49.06	3.89	13.22	13.94	9.76	4.95	0.37	0.74	3.25	0.42	39
D72B	Region 3	2415	1	20.18	90	51.39	49.17	3.86	13.24	13.69	9.94	5.05	0.28	0.71	3.22	0.43	40
D65C	Region 4	1313	1	30.75	90	30.89	48.51	2.69	15.10	10.97	11.71	6.30	0.18	0.75	3.30	0.35	51
D66A	Region 4	1711	1	30.66	90	33.17	48.67	3.33	13.59	13.31	10.75	5.79	0.16	0.57	3.12	0.33	44
D66F	Region 4	1711	1	30.66	90	33.17	49.02	3.36	13.40	12.88	10.84	5.81	0.23	0.58	3.16	0.34	45
D68A	Region 4	3103	1	36.26	90	36.38	49.72	3.31	13.70	12.41	10.47	5.80	0.24	0.56	3.10	0.33	45
D68C	Region 4	3103	1	36.26	90	36.38	49.45	3.30	13.48	12.79	10.57	5.80	0.24	0.55	3.09	0.39	45
D68D	Region 4	3103	1	36.26	90	36.38	49.73	3.32	13.53	12.74	10.39	5.74	0.18	0.57	3.10	0.33	45
RSD%							0.6	1.5	0.7	1.6	0.7	1.2	14.5	8.5	1.9	9.3	
Whole Rock																	
D54A	Region 2	743	1	5.24	91	8.94	49.16	4.01	13.11	14.25	9.58	4.89	0.35	0.75	3.43	0.48	38
D54B	Region 2	743	1	5.24	91	8.94	49.29	2.84	14.84	11.31	11.53	6.26	0.19	0.53	2.93	0.29	50
D69B	Region 3	2425	1	27.10	90	38.54	46.83	1.19	13.97	9.03	12.21	13.14	0.18	0.85	2.43	0.17	72

Table 3. (continued)

Sample	Location	Depth, m	Latitude, deg S	Minutes	Longitude, deg W	Minutes	Si O_2	Ti O_2	Al_2 O_3	FeO*	CaO	MgO	MnO	K_2O	Na_2O	P_2 O_5	Mg#
D69F	Region 3	2425	1	27.10	90	38.54	49.71	2.74	14.41	11.75	11.15	6.16	0.24	0.69	2.84	0.30	48
D71A	Region 3	2059	1	20.98	90	43.48	47.54	2.31	16.89	10.66	9.45	8.69	0.30	0.82	3.06	0.29	59
D73A	Region 3	1440	1	14.86	90	48.19	48.82	2.22	15.93	10.69	12.33	6.42	0.19	0.51	2.65	0.23	52
D66B	Region 4	1711	1	30.66	90	33.17	46.10	3.10	14.47	12.70	10.96	5.69	3.15	0.66	2.77	0.40	44
D67A	Region 4	2471	1	34.09	90	35.33	48.71	4.07	12.93	14.55	10.27	5.32	0.24	0.65	2.84	0.41	39
D67B	Region 4	2471	1	34.09	90	35.33	48.68	4.04	13.20	13.93	10.43	5.46	0.30	0.61	2.94	0.41	41

[a] Major element oxides are given in wt.%.

averaging ~2° (Tables 1 and 2). All of the surfaces have low, nearly uniform backscatter, suggesting they are sediment-covered (Figure 6a). Lobate fronts of lava flows are visible on several of the Region 2 terraces (Figure 3 and, e.g., points c and e in Figure 6a), and several of the escarpments have a mottled texture that is characteristic of pillow flow fronts (Figure 3). Several cones <50 m high (a few with craters) on the uppermost terraces are interpreted to be eruptive vents (Figure 2c and point d in Figure 6a).

3.3. Region 3: Terraces Between Sierra Negra and Floreana

[15] Region 3 comprises 16 terraces, which are systematically larger than those in Region 2 (Figure 6b and Tables 1 and 2). The tops of Region 3 terraces slope gently (average ~2°; Tables 1 and 2) to the southwest and have moderate reflectivity. With the exception of the uppermost escarpment, which is 1100 m high, the escarpments in this region range from 140 m to 460 m high and have slopes from 15° to 33° (Table 1).

3.4. Region 4: Floreana Ridge

[16] Floreana Ridge extends southwest from Floreana Island to depths >3000 m (Figures 2 and 5), with an average gradient of 101 m/km. It has a distinct mottled side-scan reflectivity texture that we interpret as areas of pillowed flows. Fewer fresh glassy pillow basalts were sampled from Floreana Ridge compared to the terraces to the west, and the rocks have thicker Mn coatings, suggesting that this area is older. We interpret Floreana Ridge as a volcanic rift emanating from Floreana volcano [*Bow and Geist*, 1992; *Lyons et al.*, 2007], comparable to the submarine rifts that extend from Cerro Azul (Region 1), Fernandina [*Geist et al.*, 2006], Wolf [*Geist et al.*, 2005], and Genovesa volcanoes [*Harpp et al.*, 2003]. Floreana Ridge has no subaerial extension, similar to Wolf and Fernandina's submarine rifts [*Geist et al.*, 2006; *Glass et al.*, 2007].

3.5. Region 5: Terraces Between Floreana Island and Wittmer Seamount

[17] Nine terraces lie at water depths of >3300 m to ~2300 m between Floreana and Wittmer seamount (Figures 2 and 5). Terrace tops have low acoustic reflectivity, indicating sediment-covered surfaces, and ~1° slopes. Abundant talus has accumulated at the foot of submarine gullies that cut the uppermost escarpment in this region, which is nearly 2000 m tall.

3.6. Region 6: Wittmer Ridges

[18] Two volcanic ridges extend south-southwest from Wittmer seamount (Figures 2 and 5) and exhibit highly variable acoustic backscatter. These ridges have moderately steep axial crests, with average gradients of 122 m/km and 108 m/km. A topographic high with high sonar backscatter lies at the base of the western ridge; seismicity was recorded in the area between 2000 and 2003 (D. Toomey, personal communication, 2004).

4. Regional Trends in Terrace Morphology

[19] Terrace abundance, size, acoustic reflectivity, and terrace margin morphology vary systematically from northwest to southeast along the platform and from shallow to deep water (Figures 2 and 7 and Table 2). Abundant small terraces in the northwestern part of the region transition to fewer larger terraces in the southeastern part of the platform margin (Table 2). Thirty-five terraces make up Region 2, only 11% of which have an exposed surface area $\geq$50 km^2. Fifteen terraces exist in Region 3, 56% of which have an exposed surface area $\geq$50 km^2 (Figure 7). Only nine terraces exist

Table 4 (Representative Sample). Trace Element Contents of Dredged Lavas[a] [The full Table 4 is available in the HTML version of this article at http://www.g-cubed.org]

Sample	Location	Depth, m	Sc	Cr	Co	Ni	Cu	Zn	Rb	Sr	Y	Zr	Nb	Ba	La	Ce	Pr
D49A	Region 2	3504	34.5	162	48	78	108	110	10	337	31.1	168.8	25.4	120	17.0	39.0	5.45
D51C	Region 2	2810	37.1	160	49	76	111	132	14	292	40.8	220.4	33.6	154	22.1	50.6	7.02
D53C	Region 2	2086	30.3	120	51	109	91	137	13	289	38.1	230.3	31.7	130	21.2	49.1	6.86
D54A	Region 2	743	32.3	40	50	31	64	138	16	315	45.5	259.2	39.7	162	25.8	59.4	8.10
D54B	Region 2	743	38.7	186	61	62	94	113	11	347	35.1	191.2	28.6	111	17.7	40.9	5.65
D55A	Region 2	1000	40.0	120	49	87	101	99	9	326	26.5	140.4	22.7	111	15.0	33.4	4.60
D56A	Region 2	1444	31.9	150	44	69	107	127	11	262	34.5	196.6	30.4	114	18.4	42.3	5.90
D57A	Region 2	1633	33.7	97	47	57	118	137	11	278	39.9	217.7	33.5	122	20.7	48.4	6.87
D59A	Region 2	1897	32.8	246	43	73	88	103	9	290	29.8	153.1	23.3	110	15.5	35.8	4.98
D61	Region 3	3440	52.9	175	59	69	127	135	12	339	46.2	248.5	36.5	137	21.9	52.2	7.46
D69A	Region 3	2425	52.4	275	55	91	104	96	10	288	35.5	187.9	26.4	106	16.4	38.5	5.46
D69B	Region 3	2425	35.4	892	66	331	80	64	19	325	18.7	61.8	22.0	230	14.8	25.9	2.95
D69F	Region 3	2425	34.8	213	65	83	90	112	13	316	35.7	194.1	26.4	113	18.5	42.6	5.82
D70C	Region 3	2811	43.4	145	52	75	110	121	9	298	37.1	190.0	26.5	105	16.6	39.2	5.57
D71A	Region 3	2059	24.4	231	54	157	51	93	13	427	24.5	137.0	23.0	107	18.5	42.1	5.58
D72A	Region 3	2415	43.1	49	52	52	122	116	13	287	42.1	233.8	35.1	138	21.9	50.8	7.15
D66A	Region 4	1711	57.5	251	61	106	121	100	9	313	35.3	177.3	25.7	105	15.8	37.4	5.33
D67B	Region 4	2471	36.9	89	69	59	128	149	13	296	49.1	254.5	35.0	129	22.5	51.5	7.14
W-2			36.2	93.3	44.7	72.5	102.6	73.2	20.3	190.3	22.4	87.9	7.7	166.8	10.5	22.7	3.0
RSD%			4.4	4.0	4.1	3.4	4.6	5.2	4.7	2.0	2.5	2.8	1.7	1.3	2.7	2.7	2.1

[a] Values in ppm. Analysis of standard rock AGV also reported.

in Region 5, 56% of which have an exposed surface area $\geq$50 km^2 (Figure 7). Likewise, fewer, larger terraces occur at the bottom of each section and progress (south to north) to more numerous, small terraces at shallow depths, especially in Region 2 (Figures 2c and 4).

[20] Variations in relative backscatter across the platform can be estimated using the side-scan sonar imagery. The mean reflectivity decreases by 22% eastward along the SW platform margin (Figure 2b). This likely indicates greater sediment accumulation in the east, attributable to increasing age of platform formation eastward. Hemipelagic sedimentation rates in the area range from 4–9 cm/ka, owing to vigorous upwelling and detritus from the islands [*Lea et al.*, 2006]. In places, we see evidence of downslope streaming of erosional debris on some of the steep escarpment faces, which also contributes to the sedimentary input to the seafloor across the platform margin.

[21] Individual lava flows and characteristic flow terminus lobes can be distinguished on the surfaces and the seaward margins of most intermediate-depth and shallow terraces (Figures 3 and 6). With increasing depth and direction southeastward along the platform, individual flow margins coalesce with adjacent terraces, forming larger, laterally continuous terraces. The escarpment edges of the deeper terraces are sharper, and rough talus slopes become predominant southeastward along the platform edge (Figures 2b, 5, and 6). These features are attributed to the extent of local erosion by rockfall, which increases with age downslope and to the east.

5. Geochemistry and Petrology of SW Galápagos Platform Lavas

[22] Submarine lavas of the SW Galápagos platform are all basalts containing abundant phenocrysts and microphenocrysts of plagioclase (9–29%), clinopyroxene (<1–11%), and olivine (1–8%) in a glassy or fine-grained matrix. The glasses and most of the bulk rocks are restricted in MgO content and range between 4.89 wt.% and 6.82 wt.% (Table 3 and Figure 8). D71A and D69B lack glass and are plagioclase- and olivine-phyric whole rock samples with MgO = 8.69 and 13.14 wt.% (Figure 8).

[23] The majority of the submarine samples are compositionally indistinguishable from subaerial Sierra Negra and Cerro Azul lavas for most major and trace elements, but they are closest in composition to the Sierra Negra field on plots of Na_2O, K_2O, and K_2O/TiO_2 (Figures 8–10). Chondrite-normalized rare earth element patterns of submarine samples are light rare earth element (REE) enriched and nearly parallel, with slight Eu anomalies (Figure 10), similar to Sierra Negra [*Reynolds and Geist*, 1995] and Cerro Azul [*Naumann et al.*,

Table 5. Isotopic Data for Dredged Lavas[a]

Sample	Location	Depth, m	$^{87}Sr/^{86}Sr$	$^{143}Nd/^{144}Nd$	$^{206}Pb/^{204}Pb$	$^{207}Pb/^{204}Pb$	$^{208}Pb/^{204}Pb$
D49A	Region 2	3504	0.703386	0.512920	19.3946	15.5892	39.0620
D49A	Region 2	3504	0.703418	0.512924	19.4041	15.5966	39.0860
D50A-gl-1[b]	Region 2	3320	0.703333	0.512911	19.3631	15.5853	39.0275
D50A-gl-2[b]	Region 2	3320		0.512921	19.3652	15.5868	39.0264
D51A	Region 2	2810	0.703372	0.512907	19.4641	15.5992	39.1483
D51C	Region 2	2810	0.703430	0.512922	19.4625	15.5986	39.1439
D52	Region 2	2458	0.703414	0.512919	19.3906	15.5883	39.0569
D53B	Region 2	2086	0.703366	0.512908	19.3775	15.5903	39.0437
D53C	Region 2	2086	0.703446	0.512916	19.3068	15.5839	38.9709
D54A	Region 2	743	0.703391		19.3967	15.5925	39.0707
D54B	Region 2	743	0.703415	0.512931	19.3793	15.5915	39.0508
D55A-ol[c]	Region 2	1000	0.703367	0.512916	19.3897	15.5977	39.0837
D56A	Region 2	1444	0.703443	0.512913	19.4118	15.5927	39.0912
D57A	Region 2	1633	0.703438	0.512918	19.3714	15.5883	39.0352
D58A	Region 2	1563	0.703520	0.512915	19.3318	15.5851	38.9997
D59A	Region 2	1897	0.703419	0.512916	19.4637	15.5969	39.1365
D60A	Region 2	3117	0.703461	0.512914	19.2950	15.5810	38.9534
D62	Region 3	2607	0.703419	0.512916	19.3770	15.5862	39.0326
D64E	Region 3	3358	0.703394	0.512927	19.3757	15.5897	39.0408
D69A	Region 3	2425	0.703413	0.512928	19.3727	15.5905	39.0384
D69A	Region 3	2425	0.703445	0.512924	19.3767	15.5930	39.0483
D69B	Region 3	2425	0.703449	0.512953	19.8252	15.6405	39.5474
D70A	Region 3	2811	0.703417	0.512915	19.4010	15.5934	39.0762
D70C	Region 3	2811	0.703412	0.512920	19.4020	15.5947	39.0646
D71A	Region 3	2059	0.703327	0.512958	19.3500	15.5887	39.0108
D72 A	Region 3	2415	0.703453	0.512927	19.4046	15.5896	39.0710
D66A	Region 4	1711	0.703418	0.512952	19.3724	15.5924	39.0346
D66F	Region 4	1711	0.703368	0.512925	19.3706	15.5922	39.0332
D67B	Region 4	2471	0.703419	0.512931	19.3952	15.5940	39.0437
D68B	Region 4	3103	0.703405	0.512927	19.3936	15.5930	39.0313

[a] Sr isotopic values are normalized to an NBS 987 Sr value of 0.71024. Nd isotopic values are normalized to a La Jolla Nd value of 0.511847. Pb isotopic values are normalized to $^{206/204}Pb = 16.9356$, $^{207/204}Pb = 15.4891$, and $^{208/204}Pb = 36.7006$. Internal precision for Sr and Nd ratios is approximately 5–10 ppm (see text). Internal precision for $^{206/204}Pb$, $^{207/204}Pb$, and $^{208/204}Pb$ is between 15 and 60 ppm.
[b] Two splits from the same rock sample.
[c] Analysis is of an olivine mineral separate.

2002] lavas. Two samples from terraces in Region 3 have major and trace element composition similar to subaerial Floreana lavas (D69B and D71A). The nine samples collected from Floreana Ridge (dredges D65 through D68) resemble subaerial lavas from Sierra Negra rather than Floreana (Figure 8 and Table 3).

[24] The majority of the submarine samples also have isotopic compositions most similar to Sierra Negra subaerial lavas (Figure 11 and Table 5), although one has affinity with Floreana volcano and another with Cerro Azul [*White et al.*, 1993; *Kurz and Geist*, 1999; *Harpp and White*, 2001]. In $^{207}Pb/^{204}Pb$ versus $^{206}Pb/^{204}Pb$ compositional space (Figure 11c), the terrace samples plot within the overlap between Sierra Negra and Cerro Azul, but lie along a linear extension of the Floreana field. The relationship between $^{208}Pb/^{204}Pb$ and $^{206}Pb/^{204}Pb$ exhibits an almost identical pattern (Figure 11b). Subaerial lavas from Cerro Azul, Sierra Negra, and Floreana are best distinguished from one another by variations in $^{143}Nd/^{144}Nd$ with $^{206}Pb/^{204}Pb$ (Figure 11d). Samples from the terraces in Regions 2 and 3 have isotopic compositions similar to Sierra Negra but extend beyond the narrow Sierra Negra field with respect to $^{206}Pb/^{204}Pb$, with the exception of D71A, which is Cerro Azul-like, and D69B, which is Floreana-like.

[25] A single stratigraphic section through a sequence of stacked terraces from Region 2 illustrates that these submarine samples do not vary beyond the range for subaerial volcanoes in single isotopic systems, and there is no systematic change in isotopic ratio or Mg# (molar MgO/MgO + FeO*) with depth and inferred stratigraphic age (Figure 12). These data suggest that the processes of magma genesis and evolution for SW Galápagos platform lavas did not change over what we

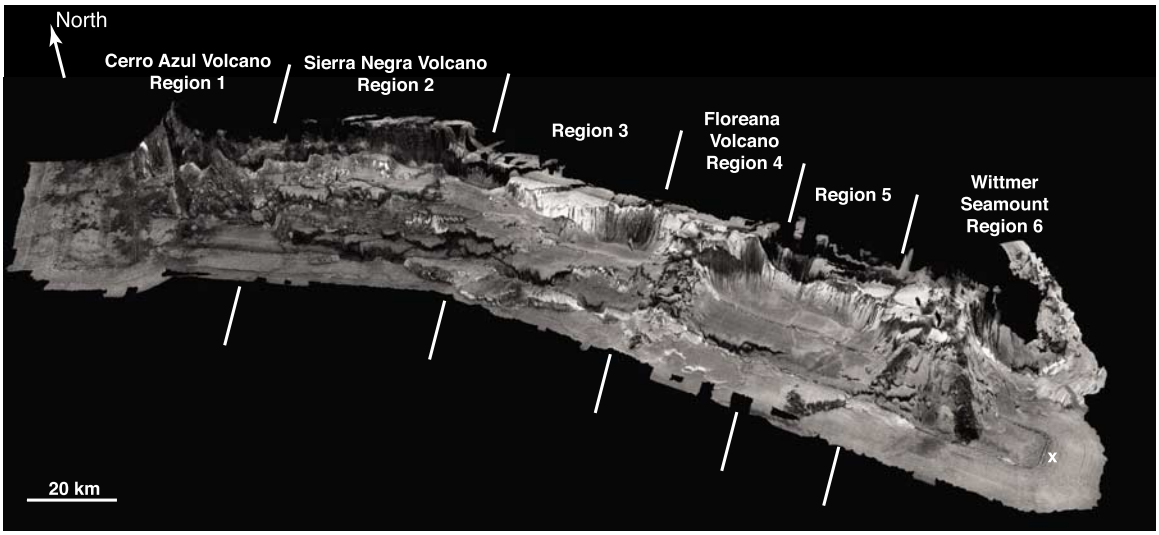

Figure 5. Three-dimensional view of the SW Galápagos platform constructed using IVS Fledermaus™ by draping side-scan sonar images over multibeam bathymetry. Perspective is from the SSE. Vertical exaggeration is 6x. The adjacent volcanic centers to the north and northeast are labeled, as are the six morphologic regions delineated on the basis of terrace morphology and primary acoustic facies. High backscatter is dark, and low backscatter is light to gray. The apparent drip-like features over the terrace edges are artifacts caused by the look angle and azimuth of the 3-D perspective and the low backscatter tops of the terraces.

estimate to be the timescale of formation of the terraces, and that the geochemical processes related to magma genesis and evolution were similar to those responsible for present-day volcanism on southern Isabela Island.

6. Discussion

[26] We consider two hypotheses for the origin of the morphology of the Galápagos terraces. The first is that the terraces formed by volcanic construction, from the eruption of many high-volume lava flows. A second hypothesis [*Chadwick et al.*, 1992; W. W. Chadwick, personal communication, 2007] proposes that the terraces are thrust blocks that originate by volcano spreading and slumping, comparable to the geologic development of the south slope of Kilauea volcano [*Chadwick et al.*, 1993; *Morgan et al.*, 2003].

6.1. Formation of Galápagos Terraces by Volcanic Construction

[27] The "shingled" acoustic reflectivity patterns, the lobate margins on some of the terrace surfaces (e.g., localities a and b in Figure 6a), the layering in some of the escarpments between terraces (e.g., locality e in Figure 6a), the occurrence of lobate flow fronts exposed in the scarps (Figure 3), and the mottled acoustic texture of some of the westernmost shallow terraces are all consistent with sequences of undeformed submarine lava flows forming each terrace. The flat tops of the terraces are then covered with a veneer of sediment. The great thickness of the individual terraces (average 330 m, with a maximum of 530 m; Tables 1 and 2) suggests that each terrace is formed by many lava flow lobes. Individual lava flows in excess of 50 m thick are undocumented in the submarine environment [e.g., *Macdonald et al.*, 1989; *Embley et al.*, 1991, 1995; *Gregg et al.*, 1996; *Chadwick et al.*, 1995, 1998; *Tivey et al.*, 1998; *Clague et al.*, 2002]. For example, lava sequences from ODP hole 504B and ophiolites are <20 m thick [*Karson*, 2002]. The largest submarine lava flow mapped at the distal end of the Puna Ridge, Hawaii, is inferred to be ~60 km long and ~5 km in width, with a maximum thickness of a few tens of meters [*Holcomb et al.*, 1988]. The deep-water lava flows of the North Arch Volcanic Field [*Clague et al.*, 2002], located >200 km north of Oahu, Hawaii are up to 80–110 km long and several tens of meters thick. Thus they may be analogs to the lava flows that make up the terraces.

[28] The uppermost scarps (those between the top terraces and the subaerial volcanoes) are higher and longer than the underlying scarps, and some have a layered structure visible in the side-scan sonar imagery (Figure 6a). These scarps are morpholog-

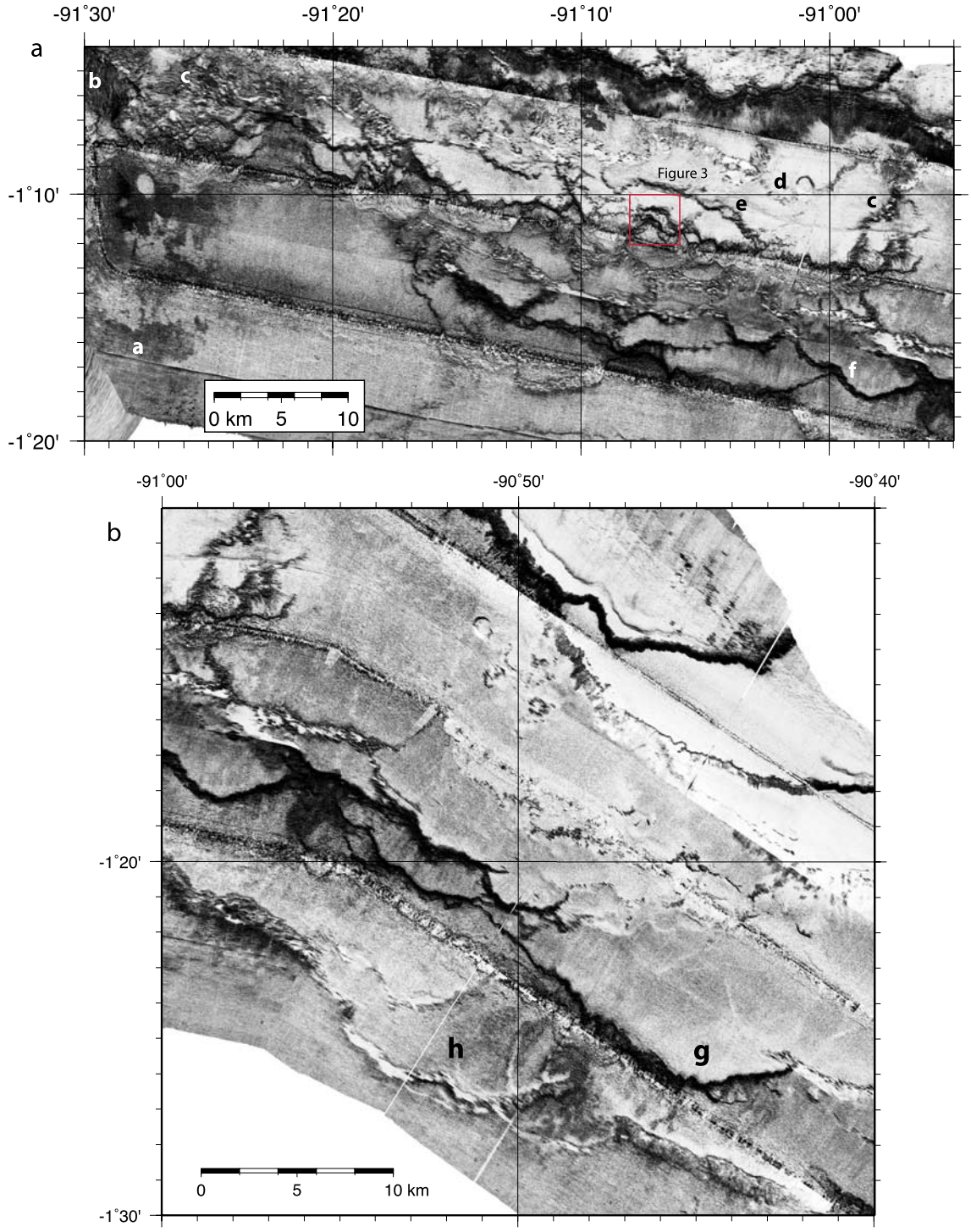

Figure 6. (a) Close-up of sonar backscatter of Regions 1 and 2 showing key morphologic features. Letters on sonar image are described as follows and discussed in the text. Point a labels deep water, large young (largely sediment free) lava flows erupted from the basal areas of the rift zones offshore Cero Azul. Points b and c label two rift zone ridges extending offshore from Cerro Azul volcano. Point d labels a shallow terrace in Region 2 offshore of Sierra Negra volcano. The small circular feature is the likely vent for the terrace-forming flows just east of point d. Point e labels well-defined lobes of flow fronts draped over next terrace level below the point d terrace. Point f labels deeper terrace in Region 2 showing a more erosionally sculpted terrace edge. The box outlines the area of Figure 3. (b) Point g identifies midlevel large terrace in Region 3 showing lower, overall acoustic reflectivity, implying greater sediment cover, but with distal margin of terrace still exhibiting lava flow front morphology. Point h indicates deep terrace in Region 3 showing erosional character of distal margin of the terrace, implying older age.

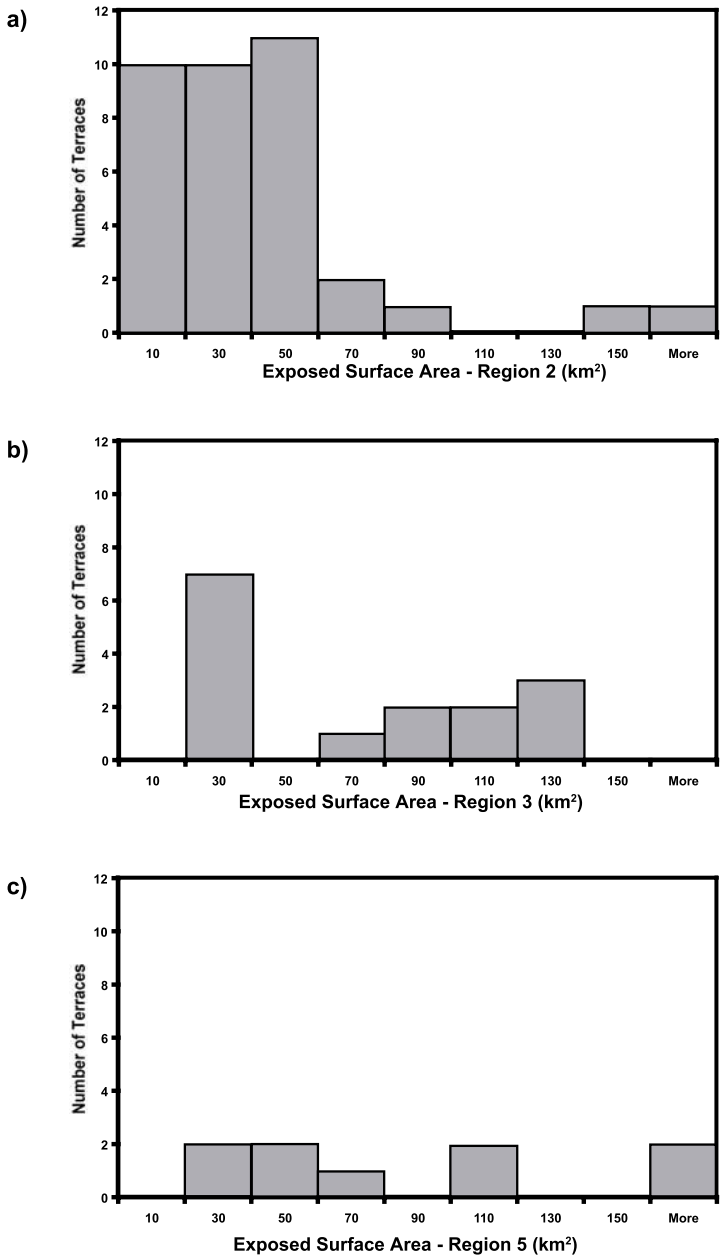

Figure 7. Histogram of exposed surface area of terraces in each of the three principal morphologic regions ((a) Region 2, (b) Region 3, and (c) Region 5), which illustrates how the frequency of terraces decreases, whereas the size, and presumed age, of terraces increases from west to east across the platform (Region 2 to Region 5).

ically similar to the uppermost submarine slopes of the west and north flanks of Fernandina volcano, which are interpreted to be sequences of lava flows that originated on land and flowed over the shoreline [*Geist et al.*, 2006]. Over time, the volcano subsided leaving the flows submerged at depths that are likely greater than their original emplacement depths. We note that high, steep scarps commonly lie seaward of the coastline of many other ocean island volcanoes, including Iceland [*Brandsdottir et al.*, 2005], Tahiti [*Clouard and Bonneville*, 2004], and Hawaii [e.g., *Chadwick et al.*, 1993], and almost certainly are due to lava flows from central volcanoes flowing into the submarine environment.

6.2. Terraces as Slumps

[29] Large-scale mass wasting of submarine flanks of oceanic islands is a fundamental feature of the

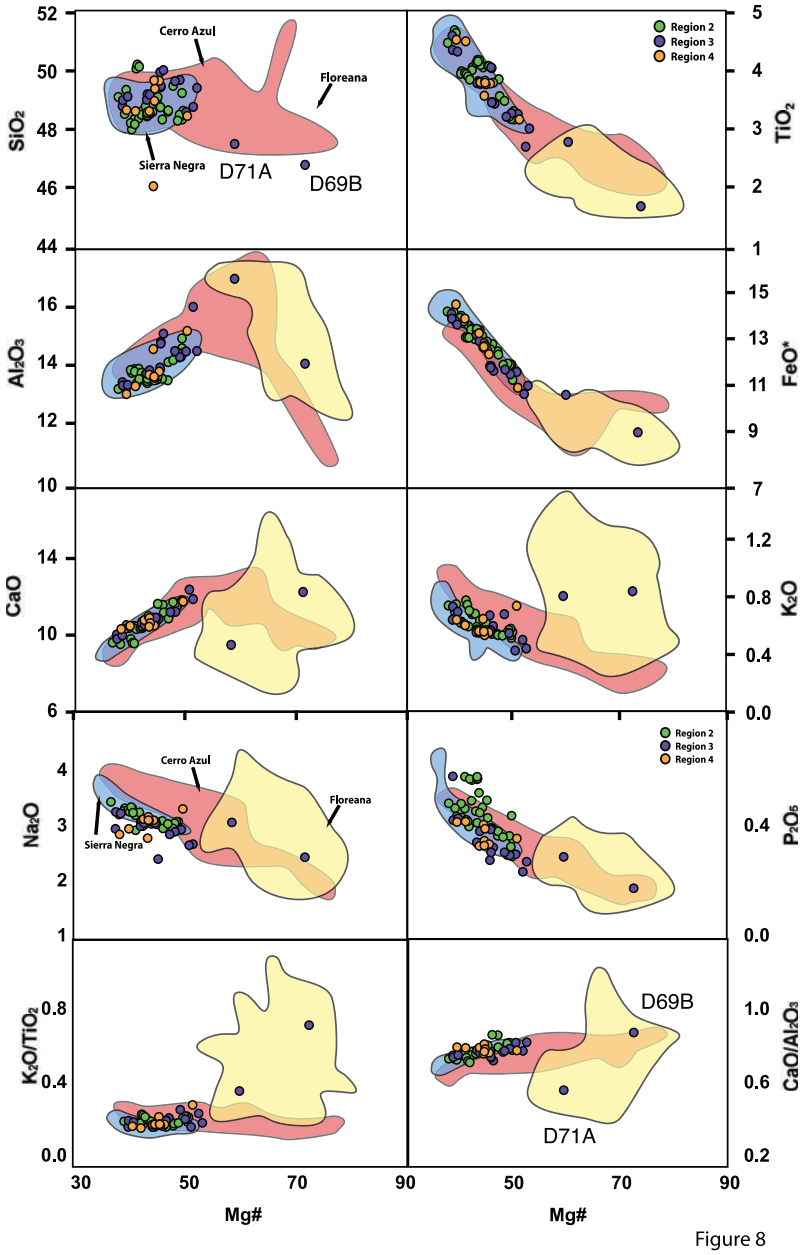

Figure 8. Major element variation in southwestern Galápagos platform glasses (symbols) compared to subaerial lavas from nearby Sierra Negra, Cerro Azul, and Floreana volcanoes [*White et al.*, 1993; *Reynolds and Geist*, 1995; *Kurz and Geist*, 1999; *Naumann et al.*, 2002; D. Geist and K. Harpp, unpublished data, 2007]. Major element data are given in Table 3.

seafloor morphology in other island chains such as the Society, Austral, Canary, Samoan, Azores and Hawaiian archipelagos [e.g., *Acosta et al.*, 2003; *Moore et al.*, 1994; *Lourenço et al.*, 1998; *Keating et al.*, 2000; *J. Smith et al.*, 2002; *Coombs et al.*, 2004; *Clouard and Bonneville*, 2004]. Mass wasting is thought to occur catastrophically, as debris avalanches associated with sector collapse of unbuttressed submarine flanks of volcanoes, or as large-scale, slow-moving slumps [*Moore et al.*, 1994]. The first process creates widely distributed deposits, which have a characteristic hummocky morphology; such deposits are absent at the foot of the SW margin of the Galápagos platform (Figures 1 and 2a). Alternatively, prominent structural features like the Hilina fault system and offshore slump deposits on Kilauea's south submarine flank move at tens of centimeters per year, sliding along

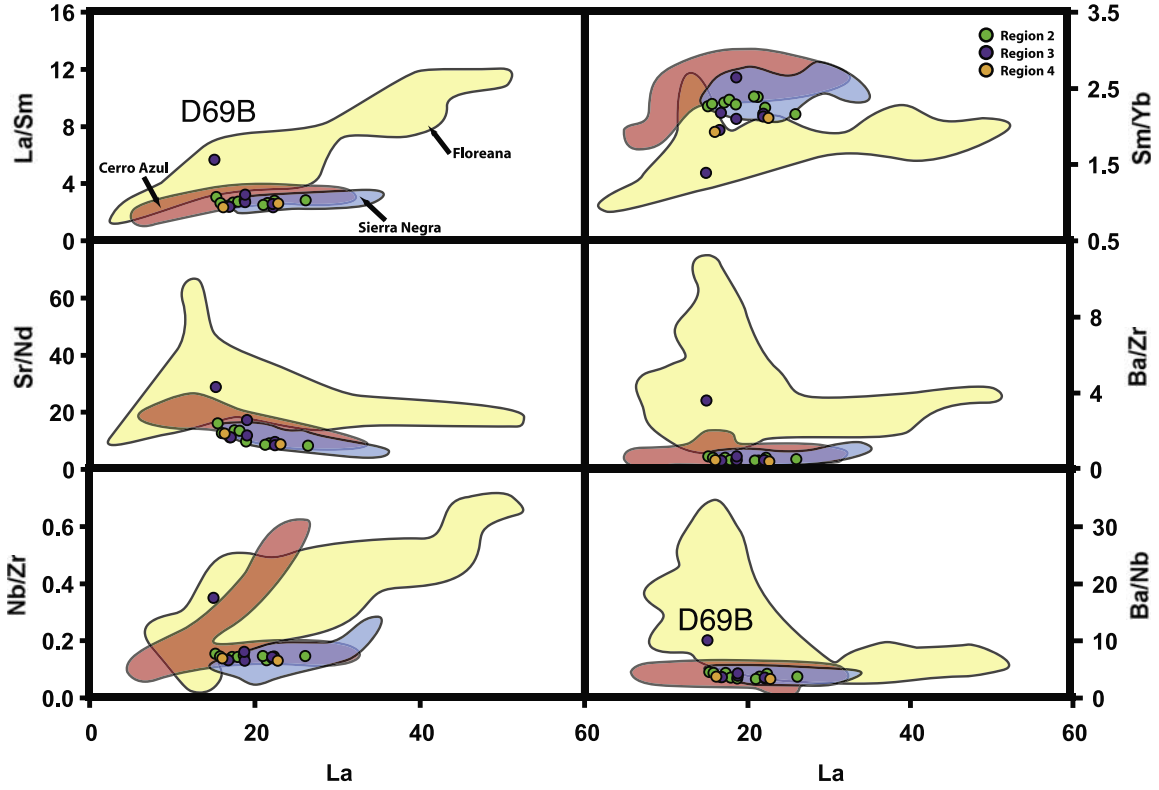

Figure 9. Trace element variation in glasses from the submarine platform suite (symbols) compared to subaerial lavas from nearby Sierra Negra, Cerro Azul, and Floreana volcanoes [*White et al.*, 1993; *Reynolds and Geist*, 1995; *Kurz and Geist*, 1999; *Naumann et al.*, 2002; D. Geist, unpublished data, 2007]. Trace element data are given in Table 4.

either a deep-seated decollement [*Lipman et al.*, 1985] or a 3 to 5 km-deep detachment [*Swanson et al.*, 1976; *Morgan et al.*, 2003]. On the south flank of Kilauea, the slumping creates a concave-seaward (in plan view) normal fault at the headwall and a convex-seaward thrust system at the foot of the slump.

[30] A slump origin for the terraces is inconsistent with the evidence, given the important differences

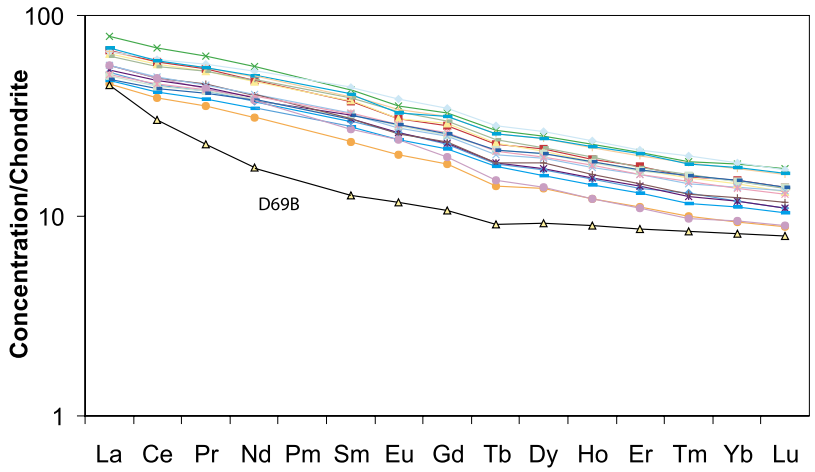

Figure 10. Chondrite-normalized REE diagram of lavas from the submarine platform suite. Chondrite normalization values are from *McDonough and Sun* [1995].

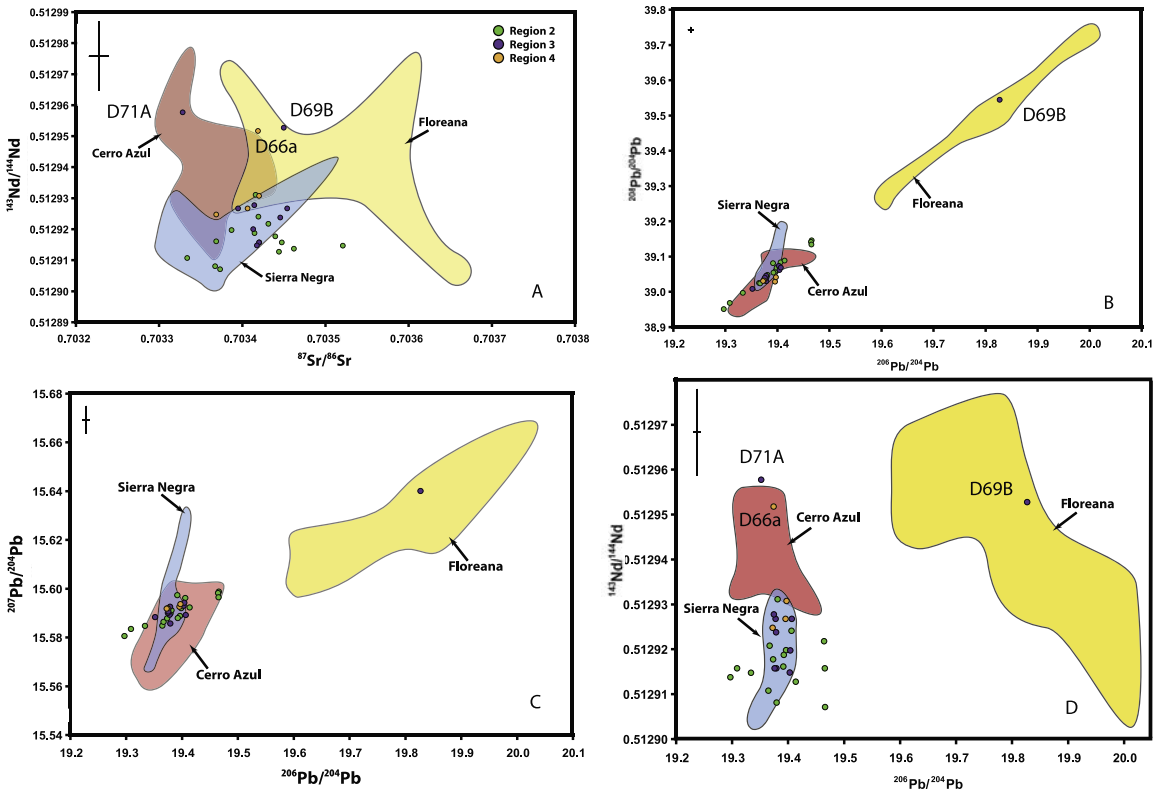

Figure 11. Isotopic composition of lavas, glasses, and one olivine separate from the submarine platform suite (colored circles) compared to subaerial lavas from nearby Sierra Negra, Cerro Azul, and Floreana (data compiled from *White et al.* [1993], *Reynolds and Geist* [1995], *Kurz and Geist* [1999], *Naumann et al.* [2002], *Blichert-Toft and White* [2001], and D. Geist and K. Harpp (unpublished data, 2007)). Isotopic data are given in Table 5. (a) Sr and Nd isotopes. (b and c) Pb isotopic compositions. (d) Covariation of Nd isotopic ratios and $^{206}Pb/^{204}Pb$ is the most distinctive among the subaerial volcanoes. Although the terrace lavas have the Nd isotopic composition of Sierra Negra, they have a slightly wider range in $^{206}Pb/^{204}Pb$.

between known slumps on the submarine flanks of ocean-island volcanoes and the SW Galápagos terraces. First, the geomorphic equivalent to a Galápagos terrace on Kilauea is what has been termed the "mid-slope bench" by *Lipman et al.* [2002] and *Morgan et al.* [2003]. Kilauea's mid-slope bench is actually a basin, formed by rotation of the thrust blocks during slumping [*Morgan et al.*, 2003]. In contrast, all Galápagos terraces slope seaward at shallow angle. The outside edge of the Kilauea's mid-slope bench is a transverse ridge, formed by anticlinal folding at the tip of thrust faults at the front of the Hilina slump [*Morgan et al.*, 2003]. We observe that Galápagos terraces slope gently and consistently to the S or SW to the upper edges of the scarps and then plunge steeply downward.

[31] The Hilina slump is bound laterally by strike-slip faults, which form between the stable part of the edifice and the hanging wall of the slump block [*Morgan et al.*, 2003]. Where the faults are oblique with respect to vergence, topographic features such as Papa'u seamount [*Fornari et al.*, 1979] result. No such lateral tears or deformational features are visible in the bathymetric and side-scan sonar maps of the SW Galápagos platform (Figures 2 and 5). The slope of the headwall at the top of the Hilina scarp is 11 to 12°, and the outer bench scarp's slope is about the same. In contrast, the scarps bounding the SW Galápagos terraces in Regions 2 and 3 are 15° to 33°. This is probably because the Hilina scarps are formed by shallow-dipping faults. Most studies of the Hilina slump present evidence that Kilauea's two strongly focused rift zones contribute to the driving force for the slump [*Swanson et*

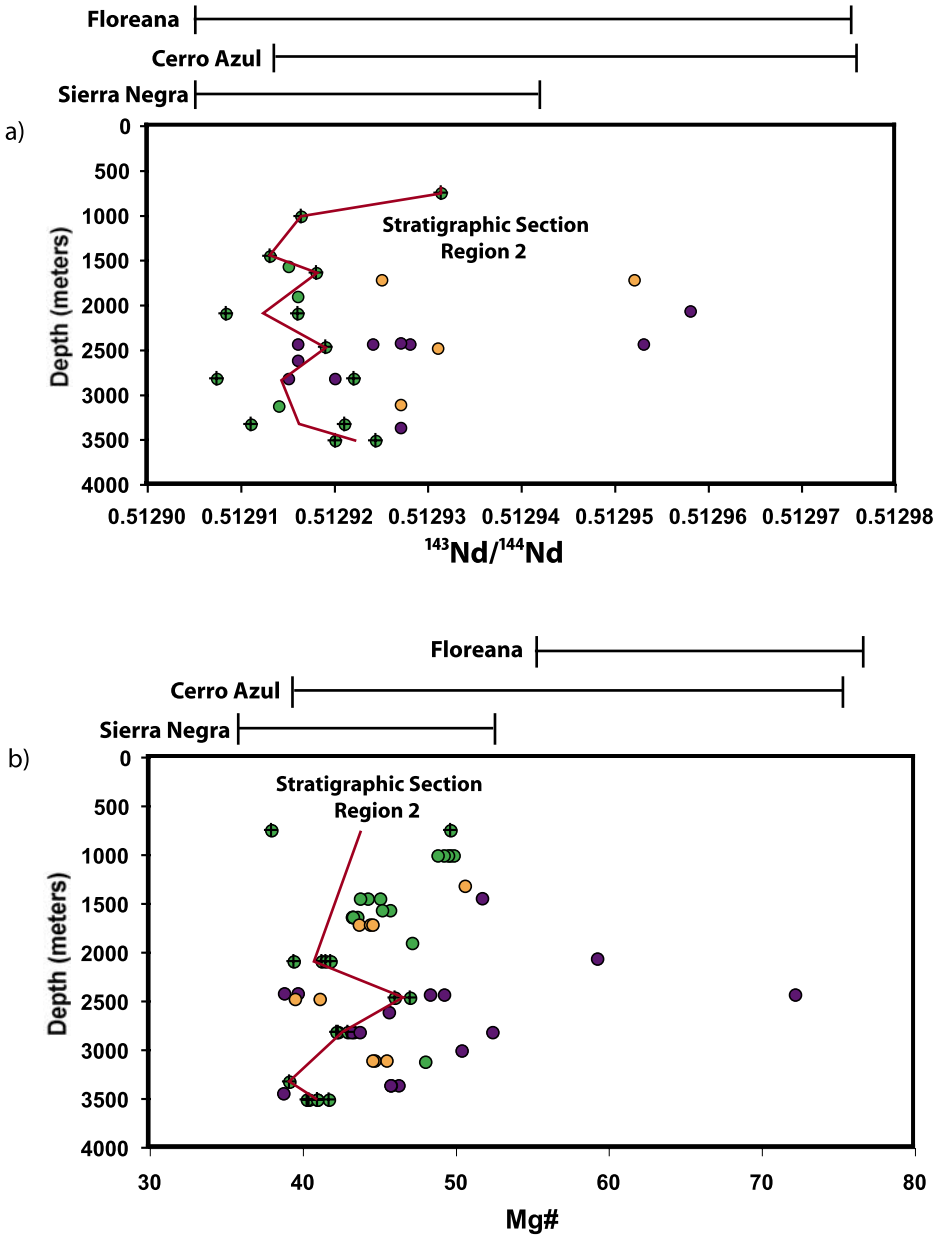

Figure 12. Nd isotopic composition and Mg# versus sample depth for submarine SW Galápagos platform lavas. Subaerial lava compositions of Sierra Negra, Cerro Azul, and Floreana volcanoes are indicated. The red line represents a single stratigraphic section through Region 2.

al., 1976; *Lipman et al.*, 1985]; Sierra Negra, Floreana, and Cerro Azul volcanoes lack focused subaerial rifts.

[32] Rocks recovered from Kilauea's mid-slope bench and outer bench high are breccias and sandstones derived from the upper submarine flank of Kilauea [*Lipman et al.*, 2002]. In contrast, none of these lithologies was dredged from the SW Galápagos terraces. Instead, the principal rock type dredged from the terrace escarpments was intact pillow lava, consistent with the interpretation of the acoustic textures as pillow lava flow fronts. For example, the feature labeled "a" in Figure 6a is likely a single lava flow front, and discrete lava flow fields occur below the lowermost scarp (Figures 2 and 3). We therefore conclude that it is unlikely that the SW Galápagos terraces are slump blocks.

6.3. Model for Formation of Galápagos Terraces

[33] We are unaware of terraces anywhere else in the Earth's oceans that are comparable in size and morphology to those that make up the SW margin of the Galápagos platform. Features analogous to the Galápagos terraces are much smaller and have been described in the submarine environment at other archipelagos, including Hawaii and the Canary Islands [e.g., *Smith and Cann*, 1999; *Clague et al.*, 2000, 2002; *J. Smith et al.*, 2002; *Mitchell et al.*, 2002]. Some of the seamounts associated with the Cobb and Bowie hot spots in the Gulf of Alaska have terraced flanks and flat tops similar in morphology to the SW Galápagos terraces but smaller [*Chaytor et al.*, 2007]. Terrace-like features are associated with volcanism with the rift valley at slow- and ultraslow- spreading MORs [e.g., *Smith and Cann*, 1999; *D. Smith et al.*, 2002; *Zhu et al.*, 2002], and lava fields whose aerial extents are comparable to those of the terraces have been described in MOR settings at the East Pacific Rise and Juan de Fuca Ridge [e.g., *Fornari et al.*, 1985; *Macdonald et al.*, 1989; *Chadwick and Embley*, 1994]. Terraces found on the flanks of the Canary Islands at depths >2000 m are only 2–5 km across, with seaward margins 100–500 m high [*Mitchell et al.*, 2002].

[34] The Azores and Iceland are perhaps the best geologic comparisons to Galápagos, because they are also near-ridge or on-ridge hot spots. The Azores are built on a platform that is similar in aerial extent to the Galápagos platform, ~500 km long and 150 km wide [*Lourenço et al.*, 1998]. The morphology of the Azores platform differs substantially from the Galápagos platform, however, as its structure is dominated by WNW and NNW fault sets, which have been attributed to slow spreading across a diffuse plate boundary between the Eurasian and Africa Plates [*Lourenço et al.*, 1998]. The available bathymetric data [*Lourenço et al.*, 1998] indicate that the margins of the Azores platform slope regularly from shallow (<1000 m) to deep (>4000 m) water. Small terraces (<5 km wide) may be present on the slopes of some of the volcanoes on the southern Azores platform, but it is difficult to tell with the existing bathymetry. The only terraced features known near Iceland are small flat-topped volcanoes around Surtsey and on Kolbeinsey ridge (B. Brandsdottir, personal communication, 2007), which are only ~1 km in diameter.

[35] The best-studied features that are analogous to Galápagos terraces are the circular flat-topped cones found on the submarine flanks of Hawaiian volcanoes. These edifices can have margins several hundred meters high [*Clague et al.*, 2000], but they have areas over 50 times smaller than the Galápagos terraces. Two mechanisms for the formation of flat-topped submarine volcanoes have been proposed: (1) Terraces grow upward and outward during the emplacement of single lava flows, by inflation from within [*Smith and Cann*, 1999], and (2) terraces form as thick ponded lavas, behind steep-sided levees constructed of pillow lavas and breccia [*Clague et al.*, 2000]; this mechanism is most effective when lava erupts from a point source at low to moderate effusion rate over a long time period. Experimental studies [*Zhu et al.*, 2002] suggest that high-viscosity lavas, gentle regional slopes, and low effusion rates support the formation of Hawaiian submarine terraces. Hydrostatic pressure and enhanced cooling of the upper crust of the lava in the submarine environment may also be important in the formation of these small-scale terraces [*D. Smith et al.*, 2002]. We propose that the SW Galápagos terraces developed by processes similar to those involved in the formation of Hawaiian flat-topped cones. The key difference is that numerous eruptions are required to construct Galápagos terraces to build the observed thicknesses and lateral contact relationships observed in the sonar data.

[36] The shingled architecture of the Galápagos terraces requires that sequential lava flows comprising each terrace must extend to similar distances from the source vents during eruptive sequences that are closely spaced in time, separated by hiatuses that permit the locus of eruption to shift and a new episode of terrace construction to begin. If sequential lava flows routinely do not reach as far as previous lava flows, a sloped surface would develop. A simple hypothesis to explain the morphology of the terraces is shown in Figure 13. It is similar to models for the formation of small lava terraces and flat-topped cones offshore of Hawaiian shield volcanoes [*Clague et al.*, 2000; *D. Smith et al.*, 2002]. In this model, the distal margins of sequential deflated lava flows must act as levees, damming the progress of subsequent lava flows (Figure 13). On the seafloor, many sheet flows deflate owing to lava draining back into the feeding system or leaking laterally [e.g., *Perfit and Chadwick*, 1998; *Clague et al.*, 2000; *Fornari et al.*, 2004; *Soule et al.*, 2007]. The flow front, which has cooled and solidified, does not deflate, leaving a restrictive lip or levee (Figure 13). Subsequent lava flows advance to the older flow front but are

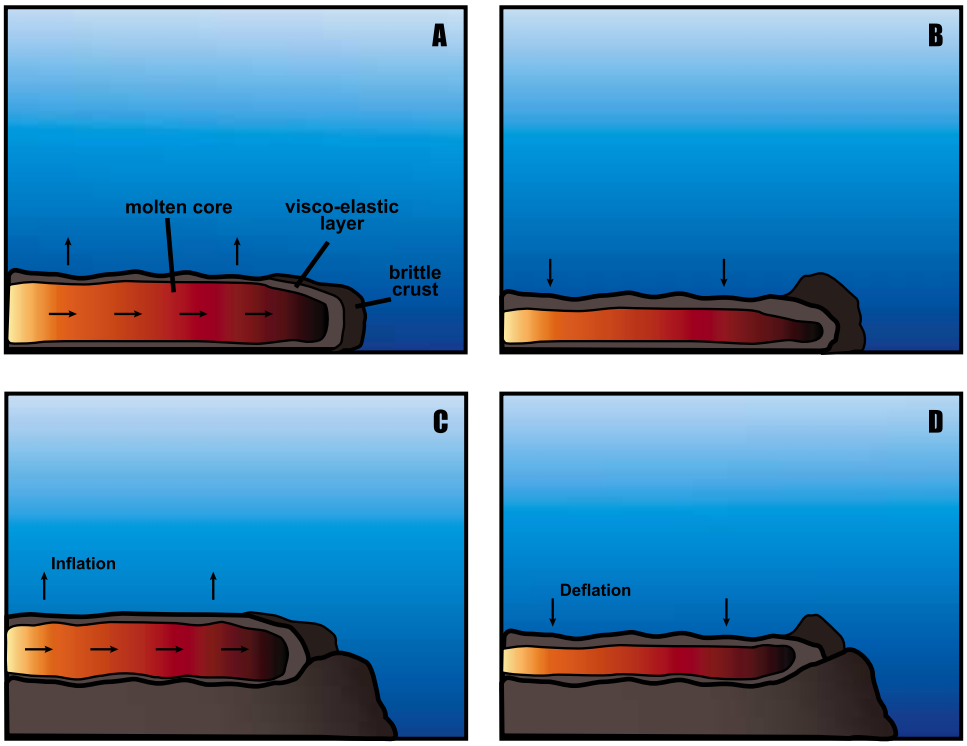

Figure 13. Deflation model as described in the text, showing the sequence for individual terrace emplacement (modified from *Clague et al.* [2002]). (a) The first lava flow advances. (b) The flow deflates due to lava drain out and/or drain-back, but brittle crust at seaward margin does not deflate because it is solid, which creates a solid lip or levee. (c) A second flow advances and is obstructed by the lava lip, thereby creating a terminus/flow front nearly consistent, spatially, with the margins of the initial flow. (d) The second flow deflates, but the brittle flow front does not, which creates another lip or levee. The sequence continues until the eruption phase stops or vent positions change, thereby building the assemblage of flows that comprise each terrace interval.

obstructed by the deflation-produced lip at the edge of the previous flow. This causes the new flow to advance to approximately the same front and inflate upward instead of advancing further. Again, lava draining laterally causes the new flow to deflate, creating another lip or levee that will restrict the advancement of successive flows. With continued eruption of lava, inflation, deflation, and the development of a lip or levee, each terrace grows upward, but the greatest lateral extent (away from the source vent) is largely constrained to the initial, voluminous outpourings that formed the foundation for each terrace interval.

[37] For the most part, source vents for the terrace-forming lava flows are not exposed. The few cones identified on the terrace surfaces are younger, small monogenetic centers (Figures 2 and 6a), and there are far more terraces than there are cones. Presumably, most of the vents responsible for forming the basal and middle sequence of terraces are buried by the shallower terraces to the north. In the case of the uppermost terraces, the lava flows likely come from the central subaerial volcanoes. On the basis of the distribution of the terraces and their morphology we suggest that the eruptions that constructed each terrace were closely timed and had similar eruptive volumes in order to have formed the continuous seaward margin of each terrace.

[38] The foundations of these submarine terraces are forming today in the western archipelago. Terraces that are morphologically identical to those of the SW Galápagos platform also exist at the youngest end of the Galápagos hot spot, between Fernandina and Cerro Azul volcanoes [*Geist et al.*, 2006]. Thus the process of terrace formation is neither restricted to the SW platform, nor is it limited to the flanks of the central volcanoes. At depths >3400 m west of the small terraces between Fernadina and Cerro Azul, voluminous ($\sim$1 km^3) flat-lying submarine lava flows $\sim$5–20 km long have been identified using the side-scan sonar data [*Geist et al.*, 2006; *Glass et al.*, 2007]. These large

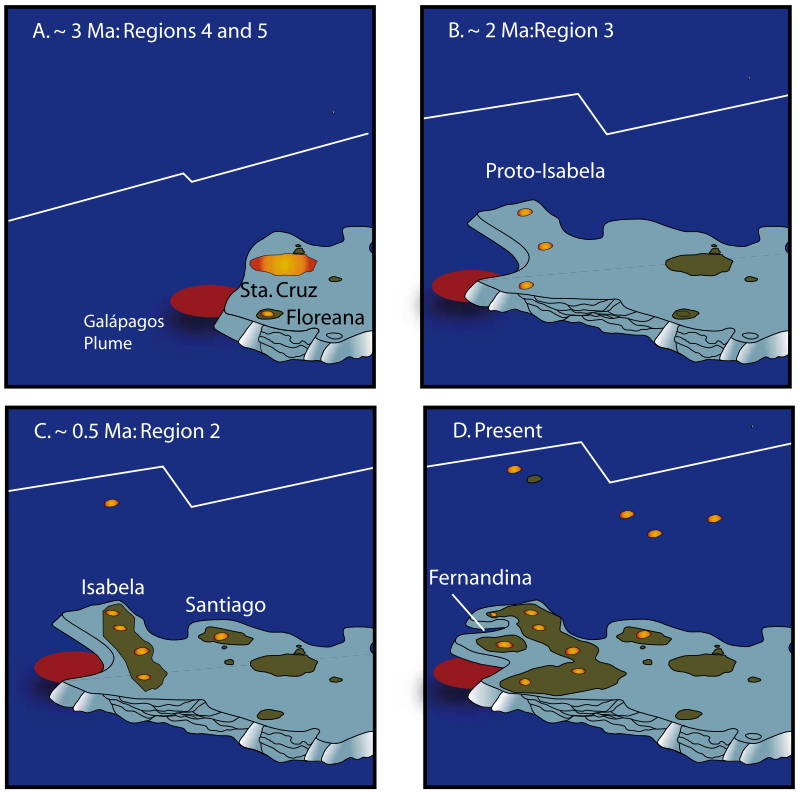

Figure 14. Evolutionary model for the Galápagos archipelago. Growth of the archipelago has been affected by the northward migration of the GSC. The archipelago alternates between phases where subaerial volcanoes grow on top of a stacked-terrace platform at the leading edge of the hot spot (e.g., ~3 Ma and 0.5 Ma to present) and other phases where only the terraces form (e.g., ~2 Ma). Note that the estimated ages of the volcanoes are conjectural.

lava flows must have been transported tens of kilometers from their source vents, across relatively flat seafloor slopes during emplacement [*Geist et al.*, 2006; *Glass et al.*, 2007], a similar setting and process to what we suggest is involved in formation of the SW platform terraces and how we envision the broad Galápagos platform has formed.

[39] The repeated northward stepping of the terraces may be caused by either cyclical decreases in the magma supply during successive terrace-building events or the northward migration of eruptive vents, with jumps back to the south to form the next sequence of terraces to the west. The migration of the GSC northward over the past 8 million years [*Wilson and Hey*, 1995] may explain the distinct increase in the size of terraces from west to east (Figure 14). The larger terraces are older, and increased magma production rates resulting from thinner lithosphere and enhanced magma supply associated with the proximity to spreading center may have resulted in the eruption of larger volume lava flows. As the GSC migrated away from the plume, magma productivity has decreased, promoting the eruption of more but smaller-volume lava flows, that characterizes the east-to-west change in dimension of the terraces.

6.4. Petrogenesis of Terrace Lavas and Tectonic Implications

[40] The compositional similarity of the lavas that make up the submarine terraces to those of Sierra Negra volcano suggest that the mantle source, degree of melting, and amount of crystallization responsible for the construction of the SW Galápagos platform have been well-regulated with time. We interpret compositional trends defined by the terrace samples as resulting from melting of the same mantle source that produces Sierra Negra magmas. Partial melt modeling by *Naumann et al.* [2002] showed that the combined compositional range of Sierra Negra and Cerro Azul lavas can be produced by 2–4% aggregated fractional melting of a garnet lherzolite source, and with the exception of Floreana-like sample D69B, the terrace

samples can be modeled with the same parameters. Only the rare earth element pattern of D69B is consistent with the absence of garnet in the source [*Bow and Geist*, 1992; *White et al.*, 1993].

[41] Conservative volume estimates for terraces along the southern platform suggest that individual terraces are composed of at least 60 km^3 of lava. If terrace lavas erupted from the center of the present archipelago, then their volumes could exceed those estimates by more than ten-fold. These large volumes may buffer the magmatic system and account for the lack of chemical variation in the platform lavas, similar to the findings at Sierra Negra [*Reynolds and Geist*, 1995], Fernandina [*Allan and Simkin*, 2000; *Geist et al.*, 2006], and Wolf volcanoes [*Geist et al.*, 2005]. The geochemical differences between subaerial and submarine Floreana reflect an important temporal evolution, which has not been observed at other Galápagos volcanoes.

[42] We propose that three evolutionary phases produce the submarine platform and subaerial volcano structure in the Galápagos archipelago (Figure 14). (1) Volcanism begins with voluminous submarine lava flows at the leading edge of the hot spot, which are supplied and erupted at a high and well-regulated rate, to build the archipelagic platform. Magma genesis and evolution are by the same processes as those that construct the subaerial volcanoes, including source compositions, the pressure and temperature of melting, and the extent of lithospheric cooling. (2) Volcanic activity coalesces episodically to form a central subaerial volcano on top of the terraced pedestal, but all aspects of magma genesis and supply remain relatively constant. (3) The progression of the Nazca plate away from the hot spot, a waning magma supply, and the production of a new sequence of terraces to the west, as well as a focusing of volcanism at a new site provide the means to expand the archipelagic platform to the west. With continued magmatic activity and plate movement eastward, the process of terrace formation adjacent to Fernandina and Cerro Azul volcanoes is predicted to continue to develop terraces along the margin of these volcanoes and expand the Galápagos platform to the west and northwest.

7. Conclusions

[43] Bathymetric and side-scan sonar data from the SW Galápagos platform confirm that the platform has been constructed by volcanic processes without major modification by large-scale scale faulting or mass-wasting. The dominant morphology of the SW margin of the platform consists of large terraces that extend for >200 km. Individual terraces are voluminous, extending up to 40 km in length and 14 km in width, and individual terrace escarpments average 300 m in height. Decreasing sonar backscatter indicates the terraces are younger to the west and older to the east, consistent with the eastward direction of plate motion [*Gripp and Gordon*, 2002]. The terraces require a well-regulated and large magma supply rate to produce lava flows that extend consistently to the width of the terraces. We hypothesize that individual terraces are built by successive eruptions of lava flows that become restricted at their distal flow margins and subsequently build the individual terraces upward and laterally, maintaining characteristic flat surfaces over broad areas. Because the GSC was closer to the hot spot when the eastern terraces formed, they are more voluminous. Geochemical evidence indicates that the submarine lavas are indistinguishable from those of Sierra Negra volcano on Isabela Island. The lack of chemical variability reflects a regulated supply of magma and from constant extents of melting of a garnet-lherzolite source.

[44] The construction of the Galápagos platform by the coalescence and superposition of large terraces may be a unique phenomenon; large terraces have not been observed at other archipelagos. This conclusion begs the question: what is unique about the Galápagos that results in this characteristic geomorphic form? We suggest that the construction of the large terraces requires especially long-duration and high-volume, but low- to medium-effusion rate submarine eruptions. The coincidence of a medium-strength hot spot [*Sleep*, 1990], the proximity of the hot spot to an intermediate-spreading rate MOR, and the fast migration of that ridge away from the hot spot may all be required to create the special tectonic and magmatic environment favorable for the growth of large terraces.

Acknowledgments

[45] We thank the officers and crew R/V *Revelle* of Scripps Institution of Oceanography (SIO) for excellent support in collecting the field data. Superb at-sea acquisition and shore-based processing of sonar data by the Hawaii Mapping Research Group are gratefully acknowledged. Our work was aided by a great scientific team that included Josh Curtice, Jeremy Haney, Joe Liccardi, Rob Otto, Bob Reynolds, Paul Johnson, and Alberto Saal. SIO shipboard technical assistance by Gene Pillard, who assisted with all dredging operations,

was excellent. Uta Peckman of SIO provided exceptional support for merging multibeam data. We gratefully acknowledge the assistance of the students who participated on these cruises and helped with the watch standing and sampling operations. Thanks to Scotty Cornelius for his adept work with the microprobe. Roger Goldsmith and Adam Soule assisted with generation of sonar images. Bill Chadwick and John Mahoney are thanked for their reviews, and Vincent Salters is thanked for his editorial handling and his own scientific review of the paper. This work was supported by the National Science Foundation grants OCE0002818 and EAR0207605 (D.G.), OCE0002461 (D.J.F. and M.K.), OCE05-25864 (M.K.), and EAR0207425 (K.H.).

References

Acosta, J., E. Uchupi, D. Smith, A. Munoz, P. Herranz, C. Palomo, P. Llanes, M. Ballesteros, and ZEE Working Group (2003), Comparison of volcanic rifts on La Palma and El Hierro, Canary Islands and the Island of Hawaii, *Mar. Geophys. Res.*, *24*, 59–90.

Allan, J. F., and T. Simkin (2000), Fernandina Volcano's evolved, well-mixed basalts: Mineralogical and petrological constraints on the nature of the Galápagos plume, *J. Geophys. Res.*, *105*, 6017–6031.

Blichert-Toft, J., and W. M. White (2001), Hf isotope geochemistry of the Galapagos Islands, *Geochem. Geophys. Geosyst.*, *2*(9), doi:10.1029/2000GC000138.

Bow, C. S., and D. J. Geist (1992), Geology and petrology of Floreana island, Galápagos archipelago, Ecuador, *J. Volcanol. Geotherm. Res.*, *52*, 83–105.

Brandsdottir, B., C. Riedel, B. Richter, G. Helgadottir, E. Kjartansson, R. Detrick, T. Dahm, L. Mayer, B. Calder, and N. Driscoll (2005), Multibeam bathymetric maps of the Kolbeinsey Ridge and Tjörnes Fracture Zone, N-Iceland, *Gephys. Res. Abstr.*, Abstract 07129.

Chadwick, W. W., Jr., and R. W. Embley (1994), Lava flows from a mid-1980s submarine eruption on the Cleft Segment, Juan de Fuca Ridge, *J. Geophys. Res.*, *99*, 4761–4776.

Chadwick, W. W., Jr., J. G. Moore, C. G. Fox, and D. M. Christie (1992), Morphologic similarities of submarine slope failures: South flank of Kilauea, Hawaii, and the southern Galápagos platform, *Eos Trans. AGU*, *73*(43), 507, Fall Meet Suppl.

Chadwick, W. W., J. G. Moore, D. A. Clague, M. O. Garcia, and C. G. Fox (1993), Bathymetry of south flank of Kilauea volcano, Hawaii, *U.S. Geol. Surv. Misc. Field Stud.*, *Map 2231*.

Chadwick, W. W., Jr., R. W. Embley, and C. G. Fox (1995), SeaBeam depth changes associated with recent lava flows, CoAxial segment, Juan de Fuca Ridge: Evidence for multiple eruptions between 1981–1993, *Geophys. Res. Lett.*, *22*, 167–170.

Chadwick, W. W., Jr., R. W. Embley, and T. M. Shank (1998), The 1996 Gorda Ridge eruption: Geologic mapping, sidescan sonar, and SeaBeam comparison results, *Deep Sea Res., Part II*, *45*, 2547–2569.

Chaytor, J. D., R. A. Keller, R. A. Duncan, and R. P. Dziak (2007), Seamount morphology in the Bowie and Cobb hot spot trails, Gulf of Alaska, *Geochem. Geophys. Geosyst.*, *8*, Q09016, doi:10.1029/2007GC001712.

Christie, D. M., R. A. Duncan, A. R. McBirney, M. A. Richards, W. M. White, and K. S. Harpp (1992), Drowned islands downstream from the Galápagos hotspot imply extended speciation times, *Nature*, *355*, 246–248.

Clague, D. A., J. G. Moore, and J. R. Reynolds (2000), Formation of submarine flat-topped volcanic cones in Hawaii, *Bull Volcanol.*, *62*, 214–233.

Clague, D. A., K. Uta, K. Satake, and A. Davis (2002), Eruption style and flow emplacement in the submarine North Arch Volcanic Field, Hawaii, in *Hawaiian Volcanoes: Deep Underwater Perspectives*, *Geophys. Monogr. Ser.*, vol., 128, edited by E. Takahashi et al., pp. 65–84, Washington, D. C.

Clouard, V., and A. Bonneville (2004), Submarine landslides in French Polynesia, in *Oceanic Hotspots*, edited by R. Hekinian, P. Stoffers, and J.-L. Cheminée, pp. 209–238, Springer, Berlin.

Coombs, M. L., D. A. Clague, G. F. Moore, and B. L. Cousens (2004), Growth and collapse of Waianae Volcano, Hawaii, as revealed by exploration of its submarine flanks, *Geochem. Geophys. Geosyst.*, *5*, Q08006, doi:10.1029/2004GC000717.

Davis, R., S. Zisk, M. Simpson, M. Edwards, A. Shor, and E. Halter (1993), Hawaii Mapping Research Group bathymetric and side-scan data processing, in *Oceans '93: Engineering in Harmony With the Ocean: Proceedings*, vol. 11, pp. 449–453, IEEE Press, Piscataway, N. J.

Diefenbach, B. A. (2004), Construction of the Galápagos archipelago: Evidence from geochemical and morphologic investigations of submarine terraces from the southwestern margin of the Galápagos platform, M.S. thesis, 109 pp., Univ. of Idaho, Moscow.

Embley, R. W., W. W. Chadwick, M. R. Perfit, and E. T. Baker (1991), Geology of the northern Cleft segment, Juan de Fuca Ridge: Recent lava flows, seafloor spreading, and the formation of megaplumes, *Geology*, *19*, 771–775.

Embley, R. W., W. W. Chadwick, I. R. Jonasson, D. A. Butterfield, and E. T. Baker (1995), Initial results of the rapid response to the 1993 CoAxial event: Relationships between hydrothermal and volcanic processes, *Geophys. Res. Lett.*, *22*, 143–146.

Escartín, J., S. A. Soule, D. J. Fornari, M. A. Tivey, H. Schouten, and M. R. Perfit (2007), Interplay between faults and lava flows in construction of the upper oceanic crust: The East Pacific Rise crest 9(25′–9(58′N, *Geochem. Geophys. Geosyst.*, *8*, Q06005, doi:10.1029/2006GC001399.

Fornari, D. J., J. G. Moore, and L. Calk (1979), A large submarine sand-rubble flow on Kilauea volcano, Hawaii, *J. Volcanol. Geotherm. Res.*, *5*, 239–256.

Fornari, D. J., W. B. F. Ryan, and P. J. Fox (1985), Sea-floor lava field on the East Pacific Rise, *Geology*, *13*, 413–416.

Fornari, D. J., M. D. Kurz, D. J. Geist, P. D. Johnson, U. G. Peckman, and D. Scheirer (2001), New perspectives on the structure and morphology of the submarine flanks of Galápagos volcanoes, Fernandina and Isabela, *Eos Trans. AGU*, *82*(47), Fall Meeting Suppl., Abstract T41D-06.

Fornari, D. J., et al. (2004), Submarine lava flow emplacement at the East Pacific Rise 9°50′N: Implications for uppermost ocean crust stratigraphy and hydrothermal fluid circulation, in *Mid-Ocean Ridges: Hydrothermal Interactions Between the Lithosphere and Oceans*, *Geophys. Monogr. Ser.*, vol. 148, edited by C. R. German, J. Lin, and L. M. Parson, pp. 187–218, AGU, Washington, D. C.

Geist, D. J., W. M. White, and A. R. McBirney (1988), Plume-asthenosphere mixing beneath the Galápagos archipelago, *Nature*, *333*, 657–660.

Geist, D., T. Naumann, J. Standish, K. Harpp, M. Kurz, and D. Fornari (2005), Wolf Volcano, Galápagos Archipelago melting at the margins of a plume and a model for magmatic evolution, *J. Petrol.*, *46*, 2197–2224.

Geist, D. J., D. J. Fornari, M. D. Kurz, K. S. Harpp, S. Adam Soule, M. R. Perfit, and A. M. Koleszar (2006), Submarine

Fernandina: Magmatism at the leading edge of the Galápagos hot spot, *Geochem. Geophys. Geosyst.*, *7*, Q12007, doi:10.1029/2006GC001290.

Glass, J. B., D. J. Fornari, H. F. Hall, A. A. Cougan, H. A. Berkenbosch, M. L. Holmes, S. M. White, and G. De La Torre (2007), Submarine volcanic morphology of the western Galápagos based on EM300 bathymetry and MR1 sidescan sonar, *Geochem. Geophys. Geosyst.*, *8*, Q03010, doi:10.1029/2006GC001464.

Gregg, T. K. P., D. J. Fornari, M. R. Perfit, R. M. Haymon, and J. H. Fink (1996), Rapid emplacement of a mid-ocean ridge lava flow on the East Pacific Rise at 9°46′–51′N, *Earth Planet. Sci. Lett.*, *144*, 1–7.

Gripp, A. E., and R. G. Gordon (2002), Young tracks of hotspots and current plate velocities, *Geophys. J. Int.*, *150*, 321–361.

Harpp, K., and D. Geist (2002), Wolf–Darwin lineament and plume-ridge interaction in northern Galápagos, *Geochem. Geophys. Geosyst.*, *3*(11), 8504, doi:10.1029/2002GC000370.

Harpp, K. S., and W. M. White (2001), Tracing a mantle plume: Isotopic and trace element variations of Galápagos seamounts, *Geochem. Geophys. Geosyst.*, *2*(6), doi:10.1029/2000GC000137.

Harpp, K. S., D. J. Fornari, D. J. Geist, and M. D. Kurz (2003), Genovesa Submarine Ridge: A manifestation of plume-ridge interaction in the northern Galápagos Islands, *Geochem. Geophys. Geosyst.*, *4*(9), 8511, doi:10.1029/2003GC000531.

Hart, S. R., and J. Blusztajn (2006), Age and geochemistry of the mafic sills, ODP site 1276, Newfoundland margin, *Chem. Geol.*, *235*, 222–237.

Holcomb, R. T., J. G. Moore, P. W. Lipman, and R. H. Belderson (1988), Voluminous submarine lava flows from Hawaiian volcanoes, *Geology*, *16*, 400–404.

Hooft, E. E., D. R. Toomey, and S. C. Solomon (2003), Anomalously thin transition zone beneath the Galápagos hotspot, *Earth Planet. Sci. Lett.*, *216*, 55–64.

Jackson, M. G., and S. R. Hart (2006), Strontium isotopes in melt inclusions from Samoan basalts: Implications for heterogeneity in the Samoan plume, *Earth Planet. Sci. Lett.*, *245*, 260–277.

Johnson, D. M., P. R. Hooper, and R. M. Conrey (1999), XRF analysis of rocks and mineral for major and trace elements on a single low dilution Li-tetraborate fused bead, *Adv. X-Ray Anal.*, *41*, 843–867.

Karson, J. A. (2002), Geologic structure of the uppermost oceanic crust created at fast- to intermediate-rate spreading centers, *Annu. Rev. Earth Planet. Sci.*, *30*, 347–384.

Keating, B. H., C. E. Helsley, and I. Karogodina (2000), Sonar studies of submarine mass wasting and volcanic structures off Savaii Island, Samoa, *Pure Appl. Geophys.*, *157*, 1285–1313.

Kurz, M. D., and D. Geist (1999), Dynamics of the Galápagos hotspot from helium isotope geochemistry, *Geochim. Cosmochim. Acta*, *63*, 4139–4156.

Kurz, M., D. Fornari, and D. Geist, and Shipboard Scientific Party (2001a), Cruise Report DRIFT Leg-4 R/V*Roger Revelle* August 23 to September 24, 2001, Woods Hole Oceanogr. Inst., Woods Hole, Mass. (Available at http://science.whoi.edu/galap_rv_drft4/index.html)

Kurz, M. D., D. J. Fornari, D. J. Geist, P. D. Johnson, J. M. Curtice, D. E. Lott, K. Harpp, A. E. Saal, and U. G. Peckman (2001b), The leading edge of the Galápagos hotspot: Geochemistry and geochronology of submarine glasses coupled to new sidescan sonar imagery, *Eos Trans. AGU*, *82*(47), Abstract T42B-0938.

Lea, D. W., D. K. Pak, C. L. Belanger, H. J. Spero, M. A. Hall, and N. J. Shackleton (2006), Paleoclimate history of Galápagos surface waters over the last 135,000 yr, *Quat. Sci. Rev.*, *25*, 1152–1167.

Lipman, P. W., J. P. Lockwood, R. T. Okamura, D. A. Swanson, and K. M. Yamashita (1985), Ground deformation associated with the 1975 magnitude-7. 2 earthquake and resulting changes in activity of Kilauea volcano, Hawaii, *U.S. Geol. Surv. Prof. Pap., 1276*, 45 pp.

Lipman, P. W., T. W. Sisson, T. Ui, J. Naka, and J. R. Smith (2002), Ancestral submarine growth of Kilauea volcano and instability of its south flank, in *Hawaiian Volcanoes: Deep Underwater Perspectives*, *Geophys. Monogr. Ser.*, vol. 128, edited by E. Takahashi et al., pp. 161–191, AGU, Washington, D. C.

Lourenço, N., J. M. Miranda, J. F. Luis, A. Ribeiro, L. A. Mendes-Victor, and J. Madeira (1998), Morpho-tectonic analysis of the Azores volcanic plateau from a new bathymetric compilation of the area, *Mar. Geophys. Res.*, *20*, 141–156.

Lyons, J., D. Geist, K. Harpp, B. Diefenbach, P. Olin, and J. Vervoort (2007), Crustal growth by magmatic overplating in the Galápagos, *Geology*, *35*, 511–514.

Macdonald, K. C., R. M. Haymon, and A. Shor (1989), A 220 km^2 recently erupted lava field on the East Pacific Rise near lat 8°S, *Geology*, *17*, 212–216.

McDonough, W. F., and S. S. Sun (1995), The composition of the earth: Chemical evolution of the mantle, *Chem. Geol.*, *120*, 223–253.

Mitchell, N. C., D. G. Masson, A. B. Watts, M. J. R. Gee, and R. Urgeles (2002), The morphology of the submarine flanks of volcanic ocean islands: A comparative study of the Canary and Hawaiian hotspot islands, *J. Volcanol. Geotherm. Res.*, *115*, 83–107.

Mittelstaedt, E., and G. Ito (2005), Plume-ridge interaction, lithospheric stresses, and the origin of near-ridge volcanic lineaments, *Geochem. Geophys. Geosyst.*, *6*, Q06002, doi:10.1029/2004GC000860.

Moore, J. G., W. R. Normark, and R. T. Holcomb (1994), Giant Hawaiian landslides, *Annu. Rev. Earth Planet. Sci.*, *22*, 119–144.

Morgan, J. K., G. F. Moore, and D. A. Clague (2003), Slope failure and volcanic spreading along the submarine south flank of Kilauea volcano, Hawaii, *J. Geophys. Res.*, *108*(B9), 2415, doi:10.1029/2003JB002411.

Naumann, T., D. Geist, and M. Kurz (2002), Petrology and geochemistry of Volcán Cerro Azul: Petrologic diversity among the western Galápagos volcanoes, *J. Petrol.*, *43*, 859–883.

Perfit, M. R., and W. W. Chadwick Jr. (1998), Magmatism at mid-ocean ridges: Constraints from volcanological and geochemical investigations, in *Faulting and Magmatism at Mid-Ocean Ridges*, *Geophys. Monogr. Ser.*, vol. 106, edited by W. R. Buck et al., pp. 59–115, AGU, Washington, D. C.

Reynolds, R. W., and D. J. Geist (1995), Petrology of lavas from Sierra Negra volcano, Isabela Island, Galápagos archipelago, *J. Geophys. Res.*, *100*, 24,537–24,553.

Rongstad, M. (1992), HAWAII MR-1: A new underwater mapping tool, paper presented at International Conference on Signal Processing and Technology, Inst. of Electr. and Electron. Eng., San Diego, Calif.

Sleep, N. H. (1990), Hotspots and mantle plumes: Some phenomenology, *J. Geophys. Res.*, *95*, 6715–6736.

Smith, D. K., and J. R. Cann (1999), Constructing the upper crust of the Mid-Atlantic Ridge: A reinterpretation based on the Puna Ridge, Kilauea Volcano, *J. Geophys. Res.*, *104*, 25,379–25,399.

Smith, D. K., L. S. L. Kong, K. T. M. Johnson, and J. R. Reynolds (2002), Volcanic structure of the submarine Puna

Ridge, Kilauea Volcano, in *Hawaiian Volcanoes: Deep Underwater Perspectives*, *Geophys. Monogr. Ser.*, vol. 128, edited by E. Takahashi et al., pp. 125–142, AGU, Washington, D. C.

Smith, J., K. Satake, J. Morgan, and P. W. Lipman (2002), Submarine landslides and volcanic features on Kohala and Mauna Kea Volcanoes and the Hana Ridge, Hawaii, in *Hawaiian Volcanoes: Deep Underwater Perspectives*, *Geophys. Monogr. Ser.*, vol. 128, edited by E. Takahashi et al., pp. 11–28, AGU, Washington, D. C.

Soule, A. S., D. J. Fornari, M. R. Perfit, and K. H. Rubin (2007), New constraints on mid-ocean ridge eruption processes from the 2005–06 eruption of the East Pacific Rise, 9°46′–56′N, *Geology*, *35*, 1079–1082.

Swanson, D. A., W. A. Duffield, and R. S. Fiske (1976), Displacement of the south flank of Kilauea volcano: The result of forceful intrusion of magma into the rift zones, *U.S. Geol. Surv. Prof. Pap.*, *963*, 39 pp.

Tivey, M. A., H. P. Johnson, A. Bradley, and D. Yoerger (1998), Thickness of a submarine lava flow determined from near-bottom magnetic field mapping by autonomous underwater vehicle, *Geophys. Res. Lett.*, *25*, 805–808.

Villagómez, D. R., D. R. Toomey, E. E. E. Hooft, and S. C. Solomon (2007), Upper mantle structure beneath the Galápagos Archipelago from surface wave tomography, *J. Geophys. Res.*, *112*, B07303, doi:10.1029/2006JB004672.

White, S. M., K. C. Macdonald, and J. M. Sinton (2002), Volcanic mound fields on the East Pacific Rise, 16°–19°S: Low effusion rate eruptions at overlapping spreading centers for the past 1 Myr, *J. Geophys. Res.*, *107*(B10), 2240, doi:10.1029/2001JB000483.

White, W. M., A. R. McBirney, and R. A. Duncan (1993), Petrology and geochemistry of the Galápagos Islands: Portrait of a pathological mantle plume, *J. Geophys. Res.*, *98*, 19,533–19,563.

Wilson, D. S., and R. N. Hey (1995), History of rift propagation and magnetization intensity for the Cocos-Nazca spreading center, *J. Geophys. Res.*, *100*, 10,041–10,056.

Zhu, W., D. K. Smith, and L. G. J. Montési (2002), Effects of regional slope on viscous flows: A preliminary study of lava terrace emplacement at submarine volcanic rift zones, *J. Volcanol. Geotherm. Res.*, *119*, 145–149.